**Masters Degree in**

Nanostructured Materials for Nanotechnology Applications

# "FROM SILVER NANOSTRUCTURES TO GOLD NANOSTARS: SYNTHESIS AND CHARACTERIZATION OF TUNABLE PLASMONIC MATERIALS"

**Jesús Gaona Marín**

February 2013

# ACKNOWLEDGMENTS

I would like to express my sincere gratitude to Professor Dr. Jesús Santamaría and Dr. Jose Luis Hueso for their guidance in this Master Project as well as for their advices and recommendations.

Furthermore, I really thank them to give me the opportunity of working in an interesting and promising project in an excellent research group, where I have met excellent laboratory partners as, Iván, M.Carmen, Vanesa, Leyre and Ana. I also would like to acknowledge Maria del Mar Encabo for the development in citotoxicity-viability experiments at Hospital Miguel Servet and also acknowledge Dr. Raul Arenal for his contribution in the SERS analysis.

I would also like to express my gratitude for the help offered by Dr. Víctor S. to solve the problems and difficulties of the research work.

I have no words to express the support of my parents in my personal and professional life, but there is one special person in my life that always is looking after me, my "yaya" Carmen, thanks a lot to all my family to be proud of me; I am really proud of you, no doubts.

## ABSTRACT

Noble metal nanoparticles have attracted a great interest because of their optical and physicochemical properties depending on size, shape and composition. For that reason these nanoparticles can be used in a wide variety of applications in different fields, such as cancer therapy, drug delivery, surface-enhanced Raman spectroscopy or biological labeling. The control of the plasmon resonance maximum absorption has a paramount importance for biomedical applications and the selection of an anisotropic morphology can also enhance their sensing capabilities. Therefore, the establishment of a proper synthesis method to control both parameters can have a great interest in the Nanotechnology field.

In this study, we have focused our research on the synthesis of silver nanostructures with spherical and cubic morphology and their subsequent evolution to gold nanostructures via a seed-growth assisted mechanism. The use of different capping triblock copolymers has been also evaluated to render different kind of nanostructures. Different experimental variables (such as the capping agent type or concentration, seed type or concentration) have been explored in order to tune the morphology and optical response of the final gold anisotropic nanostructures. The nanoparticles have been mainly characterized by UV-Vis and TEM-STEM-EELS-HAADF in order to check the plasmonic maximum absorption and its correlation with the different morphologies obtained.

At the end of the work we have used our optical and morphological tuned gold nanoparticles in two different techniques, Surface enhanced raman spectroscopy in which they are used in sensing applications and Optical hyperthermia in which our nanoparticles are used as heating agents.

# CONTENTS

**1. Background……1**

1.1. Introduction to Nanotechnology ……...……...…....……..1

**2. Gold Nanostructures……..……3**

2.1. Gold Nanoparticles ……3

2.2. Anisotropic gold-based Nanostructures……..4

2.3. Capping Agents…….……..6

**3. Synthesis of Nanoparticles……..8**

3.1.1. Synthesis of silver nanoparticles……..8

3.1.2. Silver Nanocubes……9

3.2.1. Nanostars Synthesis……9

**4. Study of different reactions parameters and their influence on the nanostructures……..……10**

4.1. Reactions with Pluronic F-127……14

4.2. Reactions with Pluronic F-68……..…22

4.3. Reactions with Pluronic P-104……28

4.4. Reactions with Silver Nanocubes……35

**5. Applications……..……..40**

5.1. Surface Enhanced Raman Spectroscopy……..40

5.2. Hyperthermia……45

**6. Conclusions……..51**

# 1. BACKGROUND

## 1.1. INTRODUCTION TO NANOTECHNOLOGY

Richard Feynman was the first person that introduced the term nanotechnology in 1959 at the lecture “There’s plenty of room at the bottom”. His idea was based on the capability of manipulating individual atoms in order to build up devices at the nanoscale (Feynman, December 1959). The talk is considered to be a seminal event in the history of nanotechnology, as it inspired the conceptual beginnings of the field decades later.

The prefix nano means $1 \cdot 10^{-9}$ meters. Nanotechnology deals with structures sized between 1 to 100 nanometers in at least one dimension. It applies engineering and fabrication knowledge at atomic and molecular scale. Thus, the lower limit is defined by the basic units of matter construction. (Gordon, Lutz, Boninger, & Cooper, 2007).

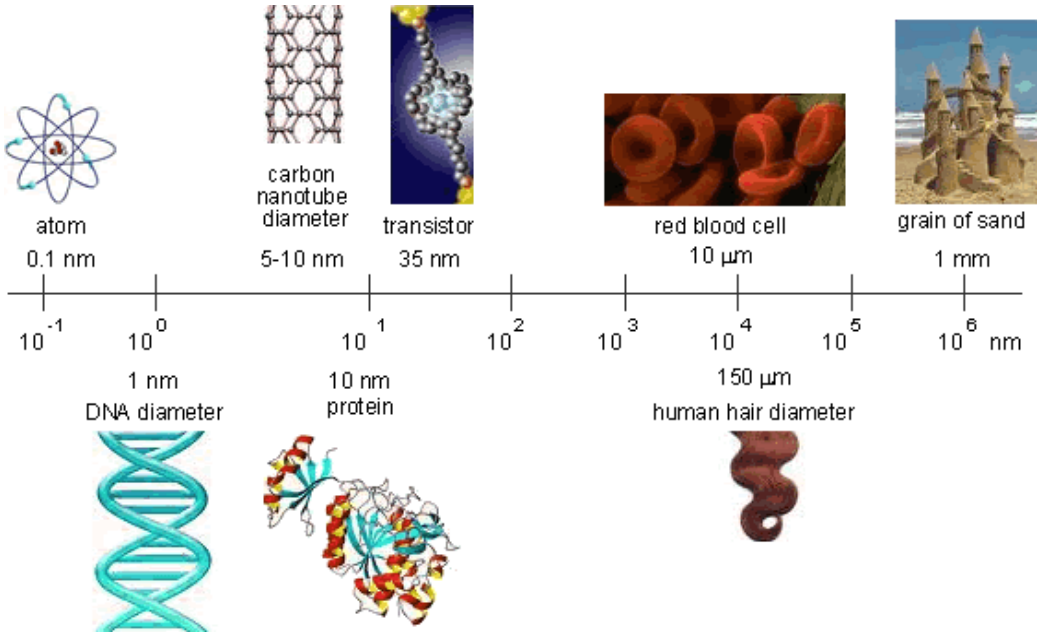


**Figure 1-1:** Nanoscale described by biomolecules, organisms, and known size objects.

Materials at the nanoscale usually show properties that are superior to and often different from the characteristics of the bulk materials. It is well known that the size and shape of the nanoparticles have a big influence on the resultant properties. For that reason, one-dimensional (have one dimension between 1 and 100 nm.) metallic nanostructures (wires, rods, stars etc) are considered as model systems to study the influence of the morphology on the mechanical, thermal and electrical properties of the nanomaterials.

Due to their special morphology star-shaped nanoparticles (multibranched nanostructures) may be particularly useful for a variety of optical, electronic, imaging, sensing, and catalytic applications due to their intrinsic properties like characteristic plasmon absorption and anisotropic chemical reactivity. The plasmonic properties of gold nanomaterials can be further tuned by exercising close control over the shape and the aspect ratio of gold nanostructures, making them useful for Near-Infrared (NIR) imaging or sensing applications. (Sperling, Ralph A., Rivera Gil, Pilar et al. 2008) and (Atwater, H. A., Polman, A. et al. 2010)

For that reason, in this study, we have focused our efforts on tuning the morphology, size and shape of gold nanoparticles using different capping ligands based on triblock copolymers. We have evaluated the influence of different experimental factors affecting the resultant nanoparticles morphologies and we have finally selected some gold nanoparticles and tested them for Surface-enhanced Raman Scattering (SERS) applications and as potential NIR photothermal agents.

# 2. GOLD NANOSTRUCTURES

## 2.1. Gold Nanoparticles

Gold is a noble metal that has been employed in several applications throughout the human history due to its properties (jewelry, decoration, curative powers…). Actually, gold in the nanoscale is an important investigation field for nanotechnology in several applications. For instance, gold nanoparticles are of interest in bioapplications owing to their assembly to biomolecules and their optical properties which strongly are related with the morphology (size and shape of the nanoparticle.)

Gold nanoparticles show a characteristic absorption band in the visible part of the spectrum which is not observed in the bulk material. The origin of this absorption is attributed to collective conduction band electron oscillation in response to the electrical field of the electromagnetic radiation of light. When the frequency of the incident light matches the intrinsic electron oscillation frequency, the particles absorb the light efficiently, resulting in the observed surface plasmon resonance (SPR) (Hao, Schatz, et al, 2004) as depicted below in Figure 2-1.

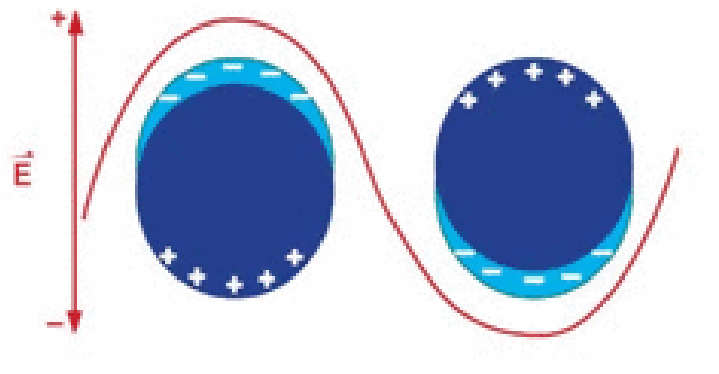


**Figure 2-1:** Schematic illustration of surface Plasmon resonance in gold nanoparticles in a polarized light field. (J.Zhang & C.Noguez 2008)

We can see in figure 2-2, the important dependence between the size and the light absorption properties. Smaller nanoparticles absorb at more energetic frequencies, for that reason we see them red colored, on the other hand bigger gold nanoparticles are blue because they absorb at less energetic wavelengths.

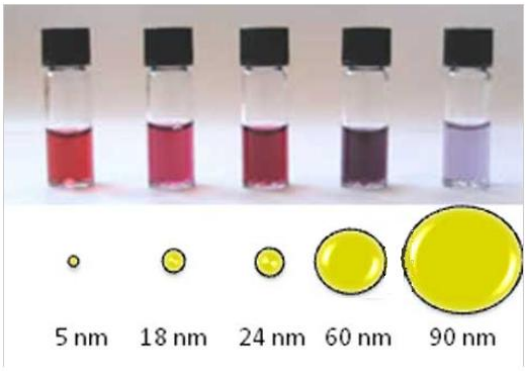


**Figure 2-2:** Solutions of gold nanoparticles with different particle size.

### 2.2. Anisotropic gold-based Nanostructures

Gold nanostars are multibranched nanoparticles with sharp tips, which due to their special morphology, display very interesting plasmonic properties that come up from the localized surface plasmon resonances (LSPR), which happens when conduction electrons in metallic nanoparticles together oscillate, as a consequence of their interaction with an in electromagnetic radiation of a concrete wavelength. (P. C.Anglomé et al.2012).

These nano-plasmonic properties of metal nanoparticles have gained an important significance due to their potential applications in fields as different as photonics, electronics, sensing or biomedicine. There is a close relationship between the optical response and the final application of the nanoparticle, for that reason is important to focus on tailoring the local surface plasmon resonance frequency range, which essentially is determined by the nanoparticle morphology. Furthermore, the excitation of a LPSR mode is related to an energy confinement at certain regions of the particles surface, forming a localized enhancement of the electromagnetic field.

As reported by Hao et al. (Hao & Bailey, 2004) when the gold tripod nanostructure is irradiated on one tip with a wavelength close to its maximum of absortion (700 nm in this case), there is an enhancement in the electric field of 3900 times the field applied (see Figure 2-3)

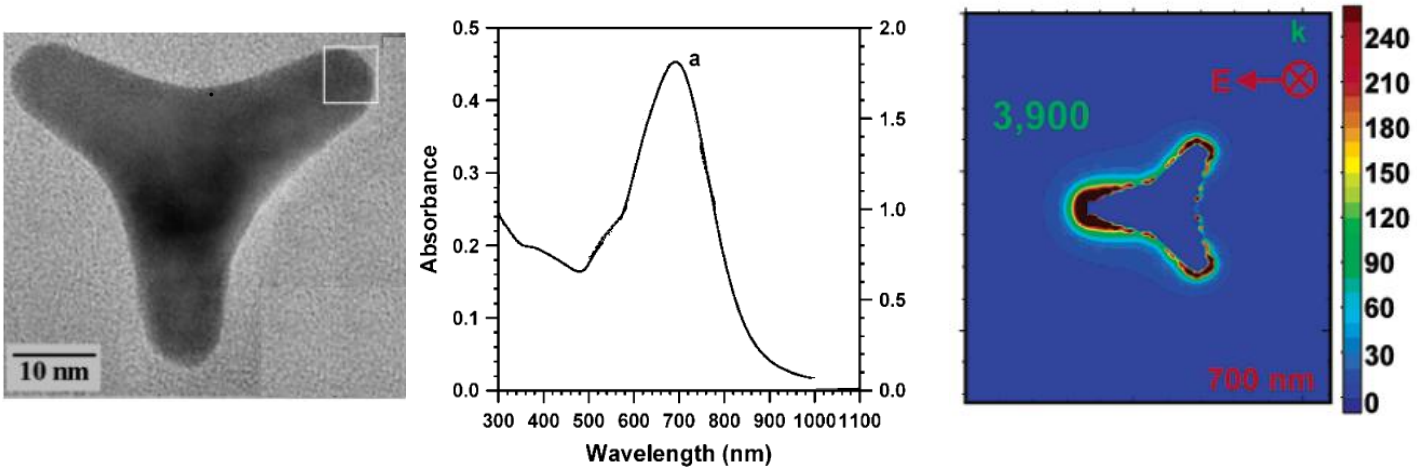


**Figure 2-3:** TEM image of a gold tripod structure, (Chen & Wang, 2003). UV-Vis absortion graph and E. Field Enhancement. (Hao & Bailey, 2004)

The localized enhancement of the electromagnetic field, is mainly given at sharp corners and edges, and also at narrow gaps, (star morphology) making particles with these kind of morphologies the object of interest for surface enhance spectroscopy techniques (S. Lal et al 2007) and (P.S. Kumar et al. 2008). For that reason, a high level of control over the synthesis of the nanoparticles is very important.

Metal nanoparticles with LSPRs in the Near Infrared (750-1300 nm) are of particular interest because tissues, blood, and water do not absorb in this spectral range, thus facilitating biomedical applications. LSPR bands in the near infrared can be achieved by increasing the anisotropy of gold nanoparticles, typically in the form of rods or stars. There are plenty of examples in the literature about synthesis of metal nanoparticles, gold in particular, where are explained protocols to synthesize nanoparticles with different sizes and shapes, so that the LSPR can be tuned in the visible and the near-infrared (NIR) region. Among them, it is worth mentioning the synthesis of gold nanostars reported by Liz-Marzán and co-workers using PVP as stabilizing agent which posses an excellent SERS detection capacity (P.S.Kumar et al. 2008) (L. Rodriguez-Lorenzo et al. 2008)

Vo-Dinh´s group has also been able to synthesize a wide variety of star-shaped gold nanoparticles with application as therapeutic and/or imaging agent (H.Yuan et al. 2011).

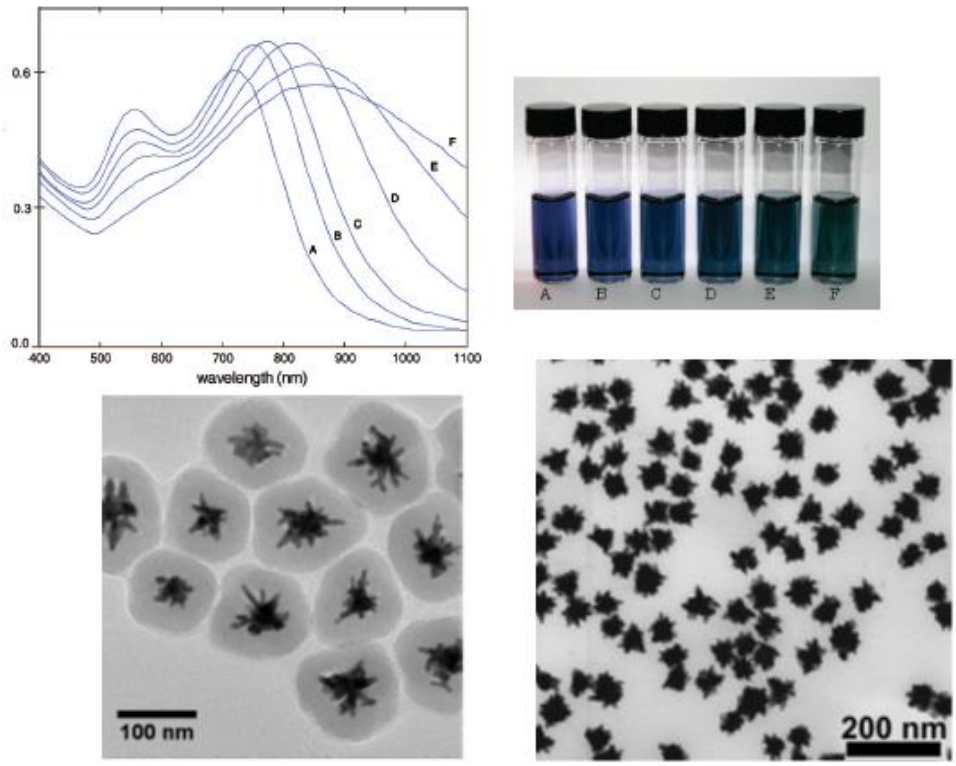


**Figure 2-4:** Absorption spectra of different sized nanostars, the size is increased from A to F, Detail of gold nanostars synthesized by Vo-Dinh and Liz-Marzán groups respectively (Khoundry and Vo-Dinh, 2008) (P.S.Kumar et al. 2008) (Andrew M. Fales et al. 2011)

### 2.3. Capping Agents

Capping agents are compounds that may favor the nanoparticle growth in some preferred orientations and also prevent agglomeration thereby rendering stable colloidal solutions. Cetyl-trimethylammonium bromide (hereafter denoted as CTAB) is a clear example of the most extended capping agents employed in the synthesis of anisotropic gold nanostructures (see chemical structure below) particularly for the synthesis of rod-shaped particles (C.J. Murphy et al 2005). Its use is also very frequent for the formation of stable micelles to generate mesoporous structures. Recently, Iqbal et al. (M. Iqbal & Yong-Il Chung 2006) reported that the combination of CTAB and the block copolymer Pluronic F-127 (See Figure 2-5 for the chemical structure) yielded gold nanorods with increased aspect ratio. Mayoral and co-workers used this combination of co-surfactants to obtain long branched gold nanostructures (Vazquez-Duran & Mayoral 2010).

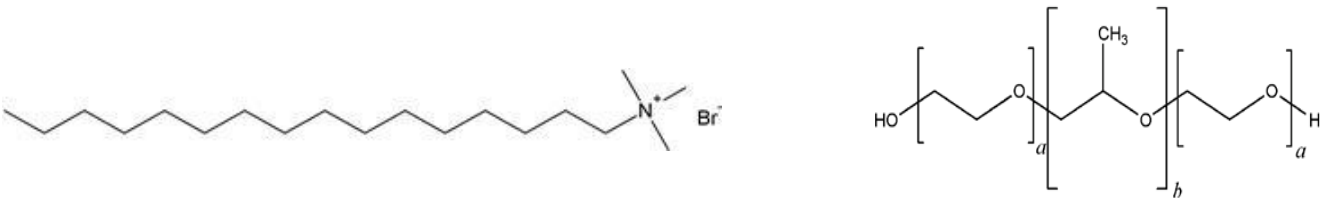


**Figure 2-5:** Structure of CTAB (left) and basic structure of Pluronic copolymers (right).

It has been demonstrated that Pluronic F-127 plays a key role as simultaneous capping and reducing agent in the formation of the long branches in gold nanostructures as shown in figure 2-6. (Álvaro Mayoral & Cesar Magen 2011).

.

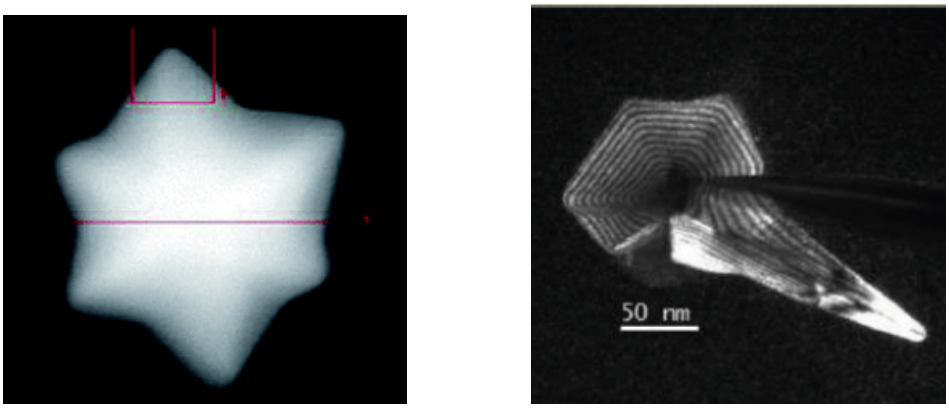


**Figure 2-6:** SEM image of a nanostructure synthesized in absence of F-127 (left) and TEM image of a nanostructure synthesized in presence of F-127 (right).

Pluronic F-127 is formed by 2 lateral chains of polyoxyethylene (PEO) and a central chain of the polyoxypropylene (PPO) (Figure 2-5). The anisotropic growth in the presence of the block copolymer is due to the hydrophobic behavior of the central chain of polyoxypropylene. Additionally, the PEO units contribute to the reduction of gold increasing the efficiency of the synthesis. (M. Iqbal & Yong-Il Chung 2006).

In the present research work, the use of Pluronic F-127 in combination with CTAB has been systematically evaluated to obtain anisotropic gold nanostructures. Moreover, additional triblock copolymers have been also evaluated to further understand the systematic role played by these types of surfactants.

# 3. SYNTHESIS OF NANOPARTICLES

All the syntheses have been carried out by a seed-growth mediated mechanism; this means that star shaped, branched gold nanoparticles have been growth from a starting solution containing metallic nanoparticles used as seeds. In our case we have utilized pseudo-spherical silver seeds and alternatively, silver nanocubes with 50-70 nm mean sizes.

### 3.1.1 Synthesis of silver nanoparticles

Silver seeds were synthesized as follows: an aqueous solution of silver nitrate $AgNO_3$ 0.25 mM was mixed with a 0.25 mM solution of trisodium citrate. Subsequently, a freshly ice-cooled solution of $NaBH_4$ 0.1 M (silver reductor agent), was rapidly added. After this addition, the solution suffered an immediate color change to dark green.

The silver seed solution was kept under static conditions for several hours prior to be used, and preserved from light in order to avoid photo-degradation.

Figure 3-1 shows the typical aspect of the colloidal solution of silver seeds, the UV-Vis spectrum with the maximum absorption located at ca. 400 nm and a TEM image of the pseudo-spherical morphology with sizes comprised between 25-100 nm

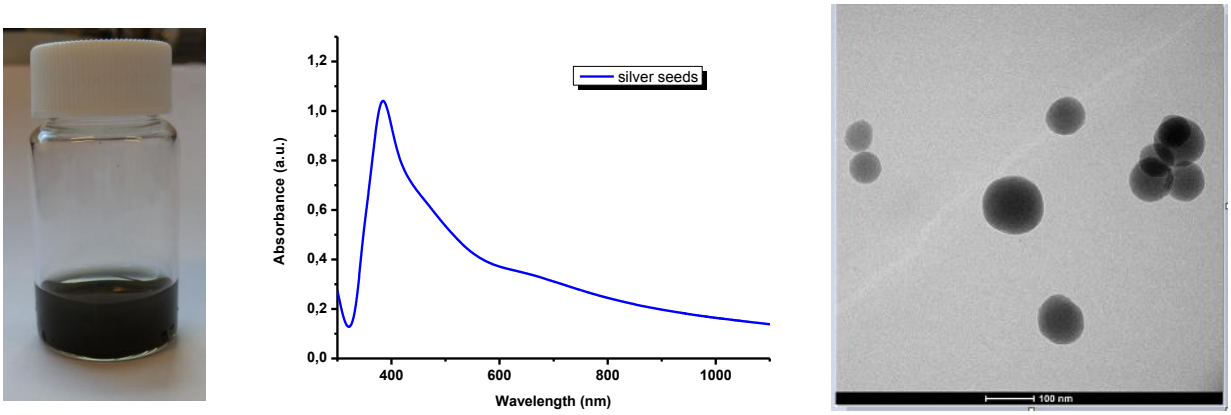


**Figure 3-1**: Digital photograph, UV-Vis spectra and TEM image of the colloidal solution containing pseudo-spherical silver nanoparticles used as seeds

### 3.1.2. Synthesis of Silver Nanocubes

Silver nanocubes were also used as seeds and were synthesized according to a synthesis protocol developed in the NFP group by Dr. Víctor Sebastián. The cubes exhibit an average size between 50 and 70 nanometers

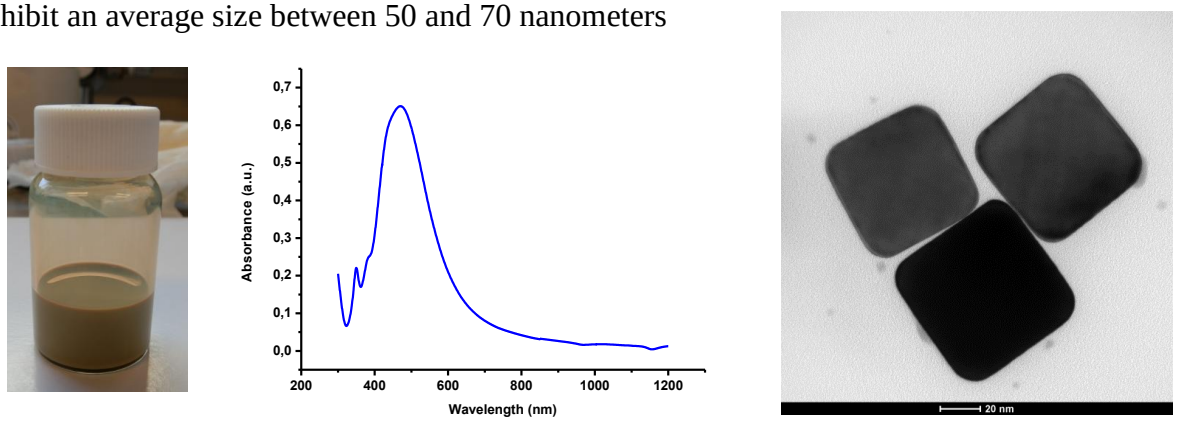


**Figure 3-2:** Digital photograph, UV-Vis spectra and TEM image of the colloidal solution containing silver nanocubes used as seeds

### 3.2.1. Synthesis of Gold Nanostars

An aqueous solution of 1.25 mM CTAB is heated and stirred until CTAB is completely dissolved. Immediately after removal of the heat source, 5 mL of $HAuCl_4$ 2.5 mM is added, forming an orange-yellow solution (Figure 3-3 a). Following, 10 mL of the corresponding triblock copolymers (F-127, F-68, P-104) are added to the mixture and stirred for 5 minutes. Subsequently, the gold ions are reduced with the addition of 0.7 mL of ascorbic acid 1 M and the solution turns uncolored (Figure 3-3 b). Finally, the seed solution is added into the reaction mixture. After 30 minutes of moderate stirring the reaction is finished. (Figure 3-3 c), then, the solution is centrifuged during 15 minutes, the supernatant is removed and the nanoparticles are redispersed in DI water.

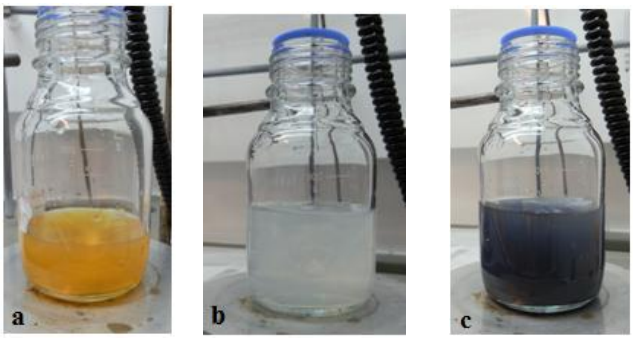


**Figure 3-3**: Digital micrographs of different moments of the nanostar synthesis.

# 4. STUDY OF DIFFERENT REACTION PARAMETERS AND THEIR INFLUENCE ON THE MORPHOLOGY AND OPTICAL RESPONSE OF THE GOLD NANOSTRUCTURES OBTAINED

The size and morphology are critical parameters, and they are closely related to the properties of the nanostructures. For that reason, it is very important to know how reaction conditions, such as, seed concentration, type of co-surfactant, temperature, etc. can influence over the resultant anisotropic star-shaped nanomaterials.

Our investigation is based on a systematic study of different synthesis modifying some parameters, in order to understand how those changes affect the nanostructures obtained.

As previously mentioned in the Introduction section, there are some references in the literature of gold nanostructures synthesized using Pluronic F-127 combined with CTAB as capping agents (M. Iqbal & Yong-Il Chung 2006) and (Álvaro Mayoral & Cesar Magen 2011). Nevertheless, a systematic evaluation of the effect of different concentrations of F-127 and other analogous triblock copolymers has not been previously addressed to best of our knowledge for the synthesis of branched and star-shaped gold nanostructures. Additionally, the effects of silver concentration and initial silver morphology have also been taken into account. Therefore, the present research work is based on the following objectives:

i) Evaluation of the effect of using different concentrations of F-127 in the presence of a low and a high concentration of silver ions, respectively.

ii) Evaluation of the effect of two different block copolymers, Pluronic F-68 and Pluronic P-104 under similar experimental conditions.

iii) Evaluation of different silver seeds morphologies varying from pseudo-spheres to cubic shapes.

All the reactions carried out in this study are summarized in the following schematic diagram. (Figure 4-1)

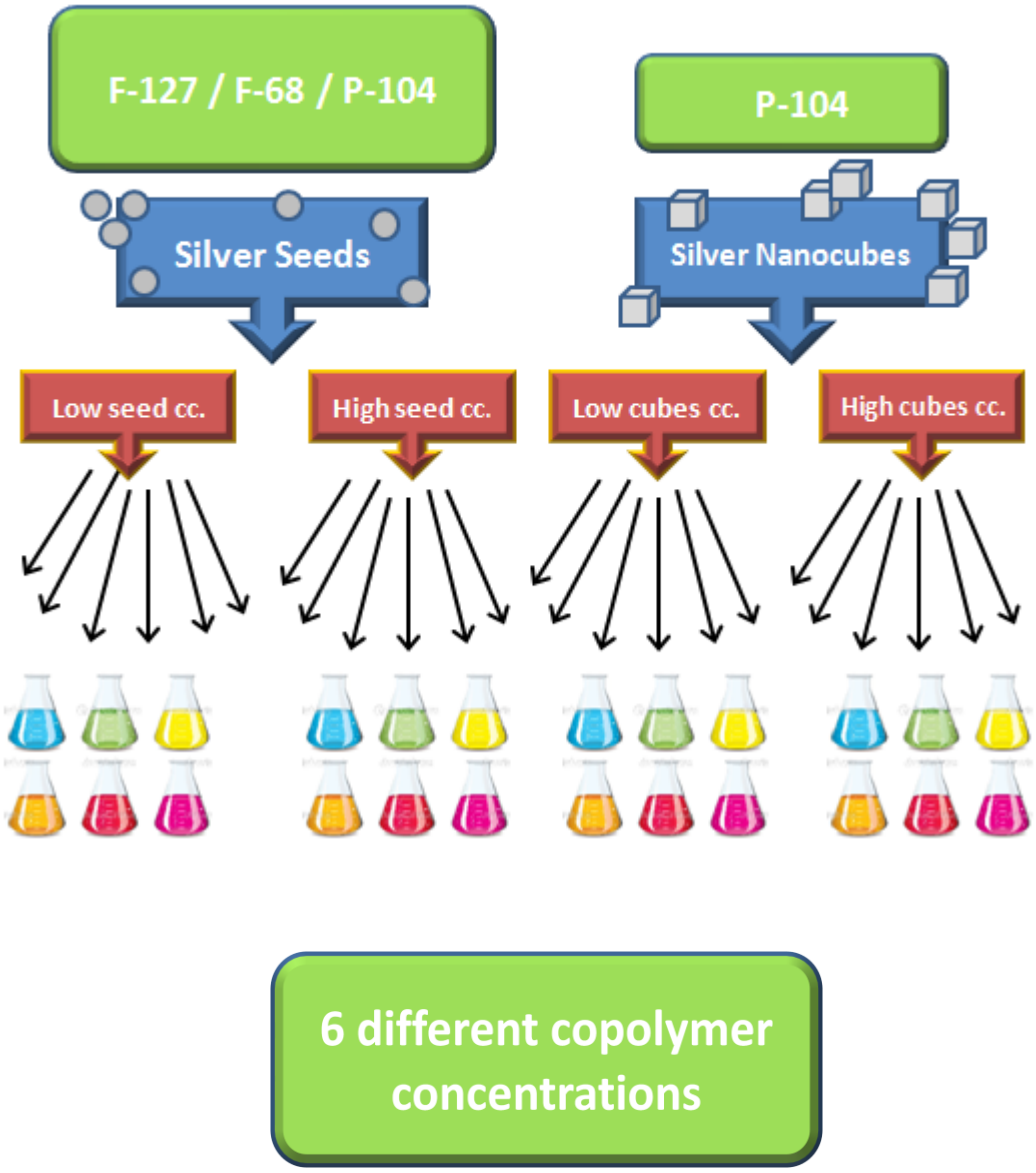


**Figure 4-1:** Schematic diagram summarizing the series of experiments carried out within the present research project

F-68 and Pluronic P-104 resemble the chemical structure of F-127, including 2 lateral chains of Polyoxyethylene and a central chain of Polyoxypropylene. Nevertheless, they have different PEO:PPO ratios and number of forming units. In the particular case of F-68, a different critical micellar concentration (CMC) value has been also reported (see Figure 4-2)

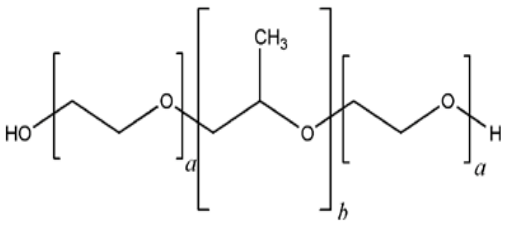


| Copolymer | a (PEO) | b (PPO) | CMC(mM) |
|---|---|---|---|
| F-127 | 100 | 70 | 0.555 |
| F-68 | 76 | 29 | 320.5 |
| P-104 | 27 | 61 | 0.508 |

**Figure 4-2**: Basic structure of Pluronic copolymers and CMC at 25 ºC of the 3copolymers used in the present study (T. Sakai and P. Alexandridis 2007)

As shown in the table contents of Figure 4-2, F-127 and P-104 have a similar CMC values reported at room temperature. Conversely, the CMC corresponding to the copolymer F-68 is 600 times higher (T. Sakai and P. Alexandridis 2007). This fact may have influence on the micelle formation, especially when working at high copolymer concentrations. Other important issue is the PEO/PPO ratio, given the preferential absorption role of PPO onto gold surfaces and the predominant reducing ability reported for the PEO units (M. Iqbal & Yong-Il Chung 2006)

The alternative copolymers F-68 and P-104 were chosen as surfactants because the former has a CMC threshold 600 times higher than F-127 and the latter has a much lower number of PEO units (see Figure 4-2). We consider that these important chemical differences can have influence on the final morphology and the plasmonic characteristics of the nanostructures synthesized with these block copolymers.

The term (S) has been defined as the molar ratio relationship between block copolymer concentration and silver seed concentration ( S = [copolymer] / [Ag] ). Consequently, higher values of S correspond to lower concentrations of seeds and vice versa.

In the reactions carried out in the presence of a high a concentration of silver seeds, the molar ratio (S) varies from 1.4 (doubling its value in each synthesis) to 45.4. In the case of reactions with low concentrations of seeds, S varies from 35.5 to 1135.2 in the same way as before. All the S values are summarized in the following table 4-1.

**Table 4-1:** Molar Ratios for different copolymer concentrations

| [Copolymer] | S at high seed cc. | S at low seed cc. |
|---|---|---|
| 0.16 mM | 1.42 | 35.5 |
| 0.33 mM | 2.8 | 70.9 |
| 0.66 mM | 5.6 | 141.9 |
| 1.33 mM | 11.3 | 283.8 |
| 2.66 mM | 22.7 | 567.6 |
| 5.33 mM | 45.4 | 1135.2 |

The rest of reactants used in the synthesis process are kept constant and their corresponding concentrations and added volumes are provided in Table 4-2.

.

**Table 4-2:** Reactants for the syntheses of gold nanostars

| Reactant | Concentration | Amount added |
|---|---|---|
| CTAB | 1.25 mM | 10 mL |
| $HAuCl_4$ | 2.5 mM | 5 mL |
| Ascorbic Acid | 1 M | 0.7 mL |

## 4.1. REACTIONS CARRIED OUT IN THE PRESENCE OF PLURONIC F-127

### 4.1.1. Experiments with high concentration of silver seeds and Pluronic F-127 as copolymer

In this section are included all the syntheses carried out with a high silver seed concentration that is kept constant and in the presence of increasing copolymer F-127 concentrations.

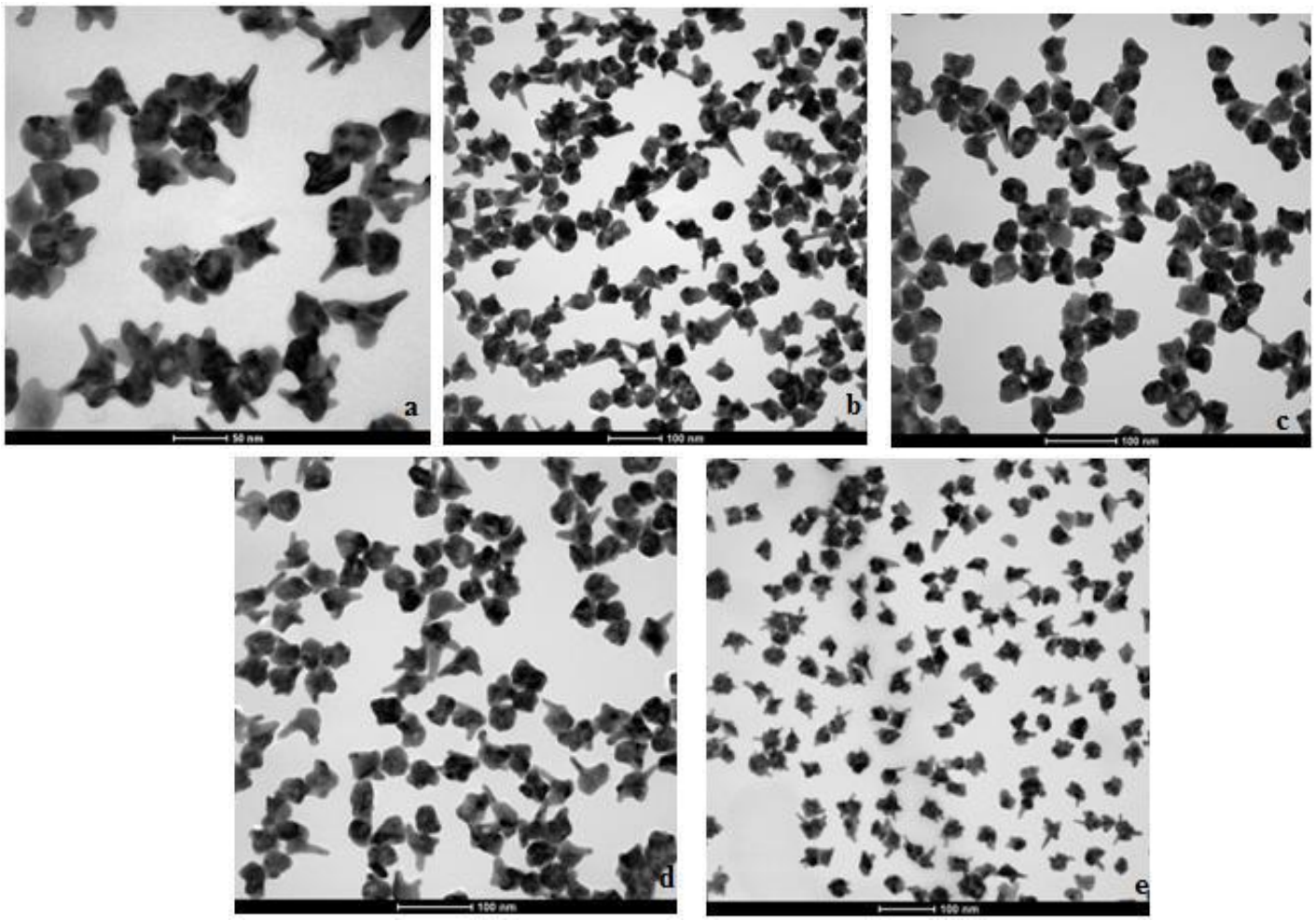


**Figure 4-3:** TEM images of anisotropic gold nanostructures synthesized at different molar ratios (S) of F-127 and high concentration of silver spherical seeds: a) S = 1.4; b) S= 5.6; c) S = 11.3; d) S= 22.7 and e) S = 45.4.

As it can be seen after the examination of the nanoparticles by TEM in Figure 4-3, the morphology remains quite similar for all the concentrations of F-127 employed. The average size is kept between 30-60 nm. These gold nanoparticles have short branches and all the samples are very homogeneous and well dispersed. Nanostructures obtained are small and contain a major number (but not significant) of branching tips as the concentration of F-127 is raised up. (Álvaro Mayoral & Cesar Magen 2011)

The evaluation of the optical response of these gold nanoparticles yields localized surface plasmon maximum absorptions between 590-620 nm (see Figure 4-4). Although the detected red-shift can be attributed to the presence of a major number of multi-branched nanostructures as we increase the ratio S, the variation is quite limited. Therefore, under these experimental conditions of elevated concentration of silver seeds, the influence of the co-polymer can be considered almost negligible.

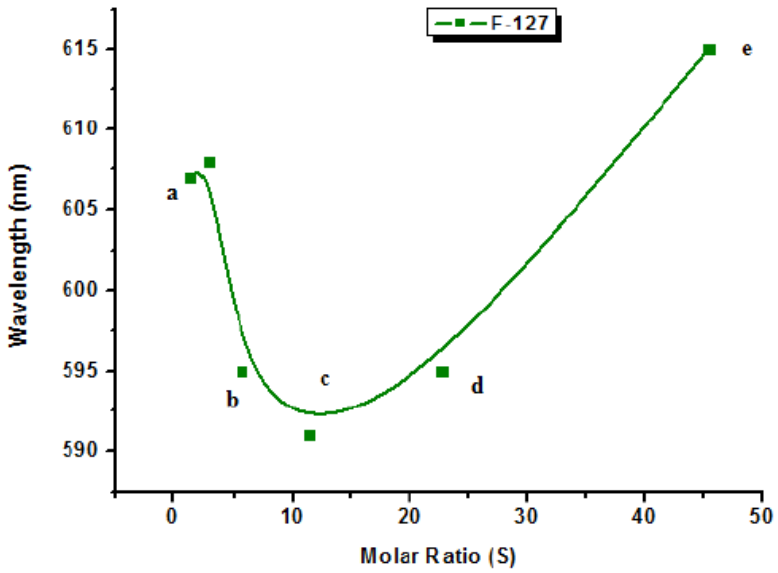


**Figure 4-4**: Evolution of the maximum absorbance obtained for increasing F-127 copolymer concentrations and high levels of silver seeds.

### 4.1.2. Experiments with low concentration of silver seeds and Pluronic F-127 as copolymer

In this section are included all the syntheses carried out with a low constant silver seed concentration (25 times lower than in the previous section) while varying the molar concentration of Pluronic F-127.)

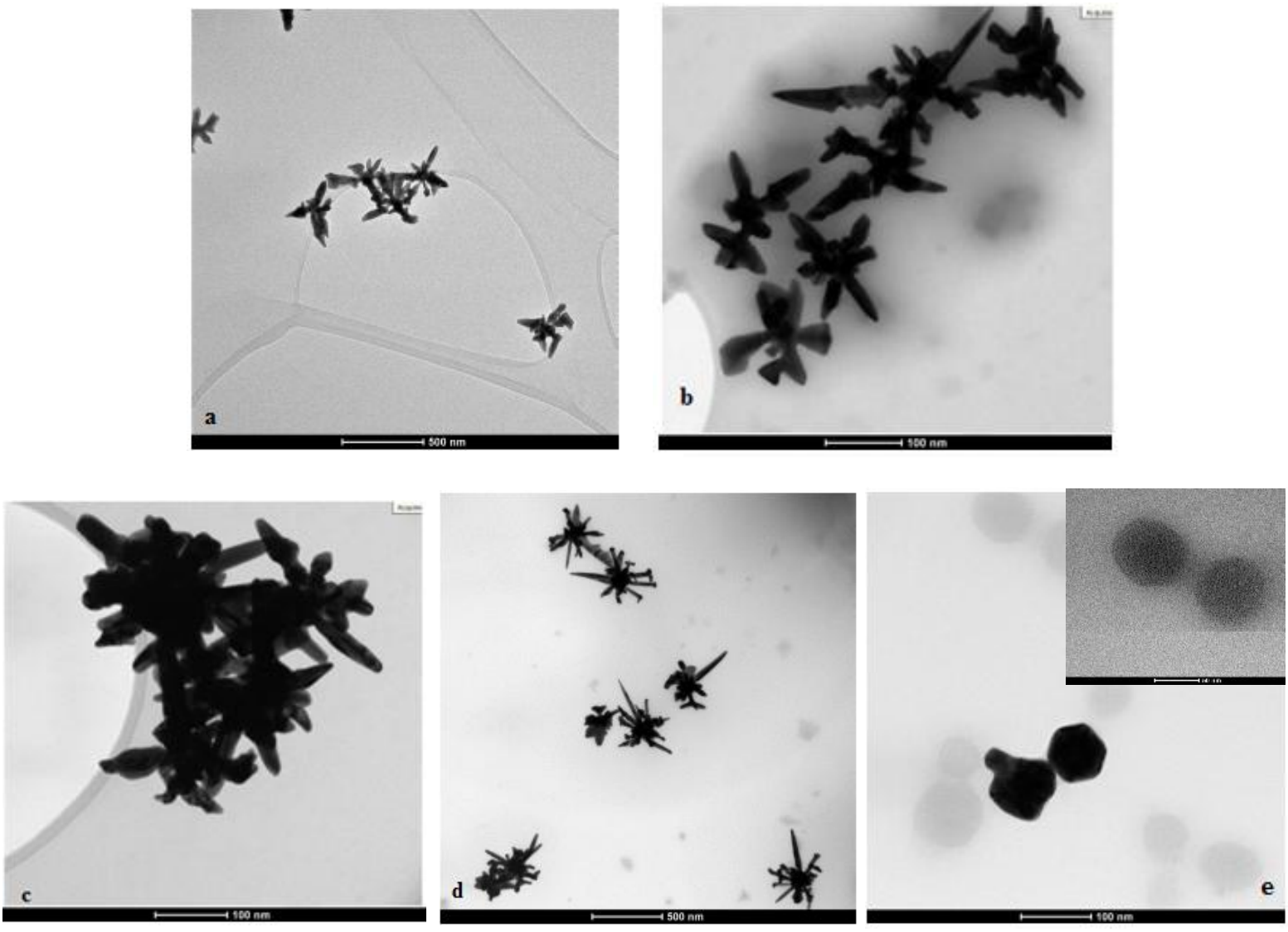


**Figure 4-5:** TEM images of anisotropic gold nanostructures synthesized at different molar ratios (S) of F-127 and low concentration of silver spherical seeds: a) S = 35,5; b) S= 141,9; c) S = 283,8; d) S= 567.7 and e) S = 1135,4.

When the ratio of silver is reduced, the influence of F-127 to obtain multibranched gold nanostructures becomes more evident, as observed by TEM in Figure 4-5.

In this case, the mean size is above 120 nm. However, there is a drastic change in the morphology in figure 4-6e corresponding to the highest S ratio (S = 1135.4) where the presence of sharped structures is depleted and only rounded gold nanostructures are obtained. It is also worth mentioning the presence of multiple micelles containing gold nanoparticles of 1-2 nm in this latter sample (see inset in Figure 4-5e).

These changes in morphology are correlated with the optical response detected by UV-Vis analysis. Figure 4-6 plots the trend of the localized maximum absorptions and shows a progressive shift to lower wavelengths in these values as we increase the ratio S.

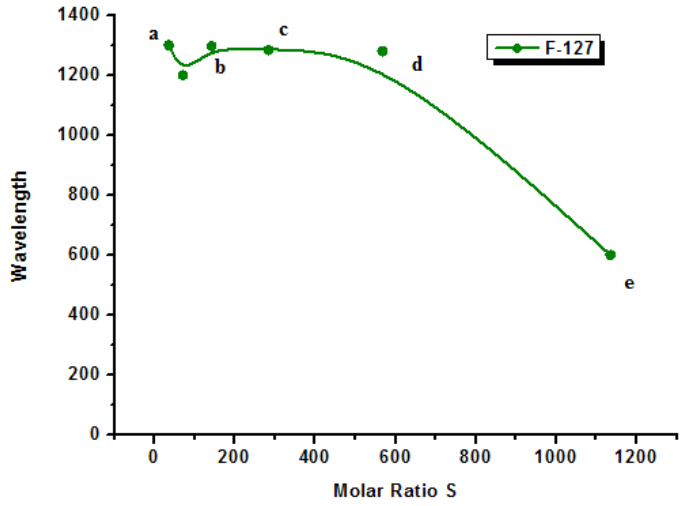


**Figure 4-6**: Evolution of the maximum absorbance obtained for increasing F-127 copolymer concentrations and low concentrations of silver seeds.

Nanoscale mapping plasmon analysis carried out by STEM-HAADF-EELS further corroborates the surface plasmon resonance enhancements located at the sharp tips of the branched nanoparticles that overlap with the maximum absorbances detected by UV-Vis (L. Rodríguez-Lorenzo et al. 2009). The blue-shift corresponding to the last synthesis can be attributed to changes in size and morphology that absorb at more energetic frequencies.

### 4.1.3. Discussion of the results obtained with F-127

Once we have finished the group of reactions in which Pluronic F-127 is present, we can extract some ideas analyzing the results:

***Influence of silver seeds concentration:***

It has been demonstrated that the concentration of silver seeds strongly influences the final sizes and morphologies of the synthesized gold nanoparticles and has a stronger influence than the change of concentration of the copolymer F-127. In our experiments, we have obtained nanostructures between 30 – 60 nanometers with a limited level of branching (See Figure 4-3). Conversely, when a low concentration of seeds is added we have synthesized long-sharped nanostructures bigger than 120 nm containing multiple thorns (See Figure 4-4).

It has been previously reported in the literature that silver seeds are oxidized by $HAuCl_4$ to silver $Ag^+$ ions in the presence of ascorbic acid according to reaction (R1) and scheme in Figure 4-7 which is known as an example of galvanic replacement (H. Yuan & W. Ma 2011). Metallic gold nanoparticles are formed and act as nucleation points. Therefore, the differences in the mean sizes account for the major number of nucleation points generated at high concentrations of silver seeds, thereby yielding smaller nanoparticles.

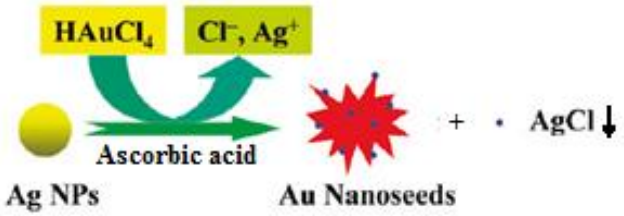


**Figure 4-7**: Reaction mechanism proposed for the gold reduction process in the presence of silver and ascorbic acid.

**R1)** $HAuCl_4\ (aq) + \text{Ascorbic Acid} \xrightarrow{\text{Ag Seeds}} Au^0 + Ag^+ + Cl^-$

**R2)** $Ag^+ + Cl^- \rightarrow AgCl\downarrow$

$Ag^+$ and $Cl^-$ ions are formed as reaction byproducts and precipitate in the form of AgCl due to the low solubility of this compound in water. (Reaction R2). As Yuan et al. claimed for their nanostars synthesis (H. Yuan & W. Ma 2011) and it is known for gold nanorods (C.J. Murphy et al 2005) AgCl can be deposited over the growing gold surfaces thereby affecting its isotropic growth and facilitating the formation of thorny and irregular shapes.

At high silver seed concentration, this effect has a stronger impact and explains the morphologies obtained. These nanostructures resemble the thorny gold nanoparticles reported by Yuan et al. (H.Yuand & W. Ma 2011) and the corresponding optical response is also compared in Figure 4-8.

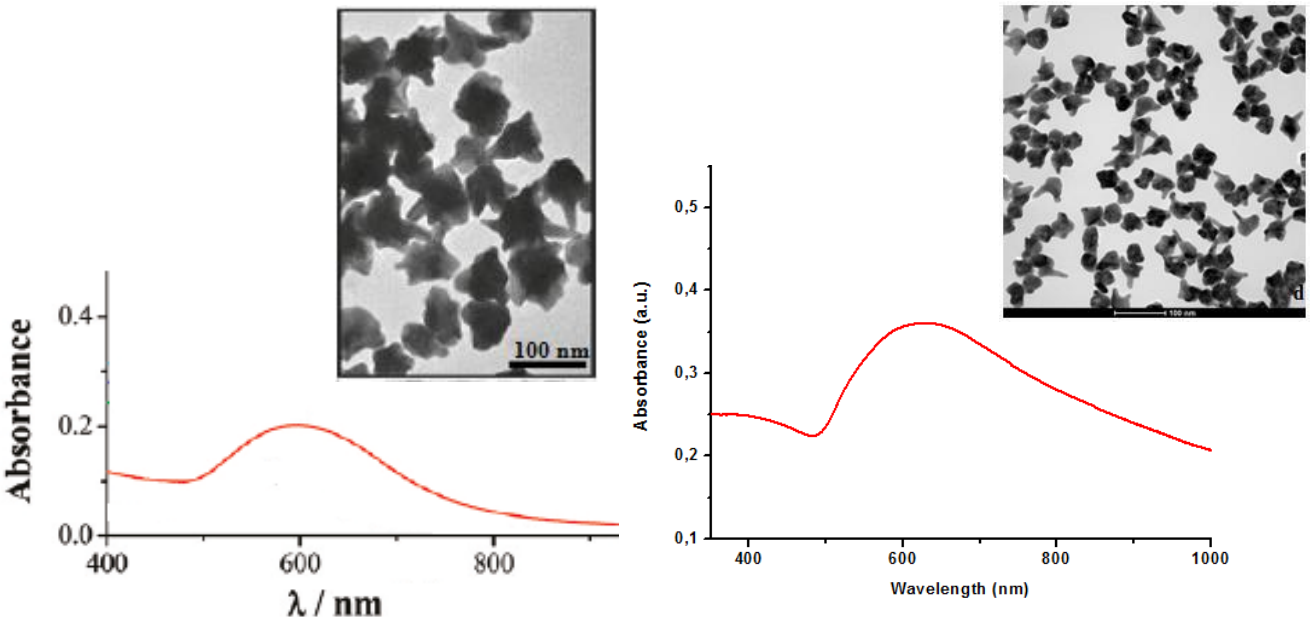


**Figure 4-8:** TEM image and UV-Vis absorption curve of thorny gold nanoparticles reported by Yuan et al. (H. Yuan & W. Ma 2011) (left) and our experimental results (right).

Hence, given the lack of variation in the morphologies even at elevated concentrations of F-127 copolymer, the formation of these AgCl layer seems to have a stronger influence that the co-directing agents.

- ***Influence of the copolymer concentration:***

It has been previously reported that F-127 molecules form stable complexes with CTAB molecules (Álvaro Mayoral & Cesar Magen 2011) and the hydrophobic PPO heads are preferentially absorbed onto the gold surfaces forming a compact CTAB-Pluronic bilayer. Figure 4-9 depicts the reaction mechanism that favors the formation of anisotropic gold structures in the presence of the copolymer and CTAB:

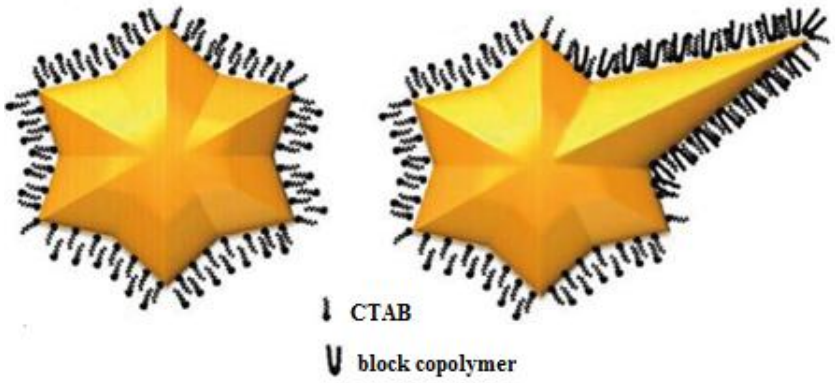


**Figure 4-9:** Schematic cartoon showing nanomaterials obtained in the absence and presence of Pluronic surfactant. (left) Original gold nanoparticle coated with a CTAB bilayer; (right) resulting branched nanoparticle stabilized with CTAB and a copolymer.

The hydrophobic tails of the CTAB bind to the relatively hydrophobic PPO blocks of the Pluronic polymer, leading to the association of CTAB with the Pluronic polymer, thus forming stable surfactant-polymer complexes (see Figure 4-9).

The use of more stable polymer-surfactant complexes by the addition of Pluronic increases the yield and the anisotropy degree of the resultant gold nanostars and increments their size. In the present series of experiments, the effect of increasing the amount of F-127 has been downsized by the leading influence of the in situ generated silver ions as described above. Only in the presence of low concentrations of silver seeds, the effect of the polymer-surfactant complexes has been clearly observed, yielding long multi-branched nanostars.

The formation of bigger nanostructures in this latter series of experiments can be justified by the lower number of nucleation points and the increased reducing capacity provided by PEO units of F-127 (T. Sakai et al. 2007). This enhanced reducing behavior was experimentally verified when the CMC threshold limit was reached. A great number of micelles containing small gold nanoparticles were detected by TEM (see Figure 4-10) and a change of morphology occurred. Therefore, the presence of the surfactant-polymer complex was not so effective due to the self-formation of copolymer micelles.

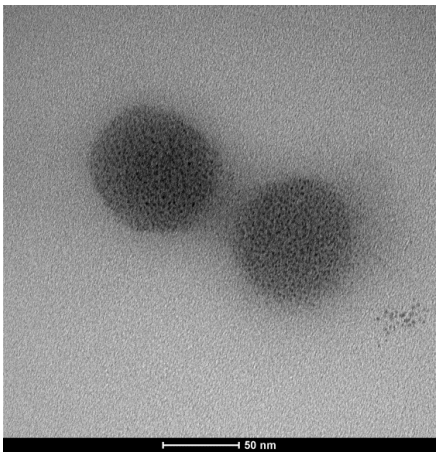


**Figure 4-10:** TEM image of a Micelle formed during a synthesis carried out with the highest concentration of copolymer Pluronic F-127 and low pseudo-spherical seed concentration

## 4.2. REACTIONS CARRIED OUT IN THE PRESENCE OF PLURONIC F-68

In this section, the same group of reactions has been carried out but replacing F-127 by Pluronic F-68. The main differences between both copolymers are based on: i) their CMC thresholds, which is 600 times higher for F-68 at 25 ºC and ii) the lower number of PEO-PPO units for F-68. (T. Sakai et al. 2007). Therefore, the formation of micelles should be prevented even at high concentration of copolymer.

### 4.2.1. Experiments with high concentration of silver seeds and Pluronic F-68 as copolymer

The following figures correspond to syntheses carried out using Pluronic F-68 as surfactant. Figure 4-11 show the morphological evolution of the gold nanostructures obtained with the variation of the concentration of F-68 copolymer.

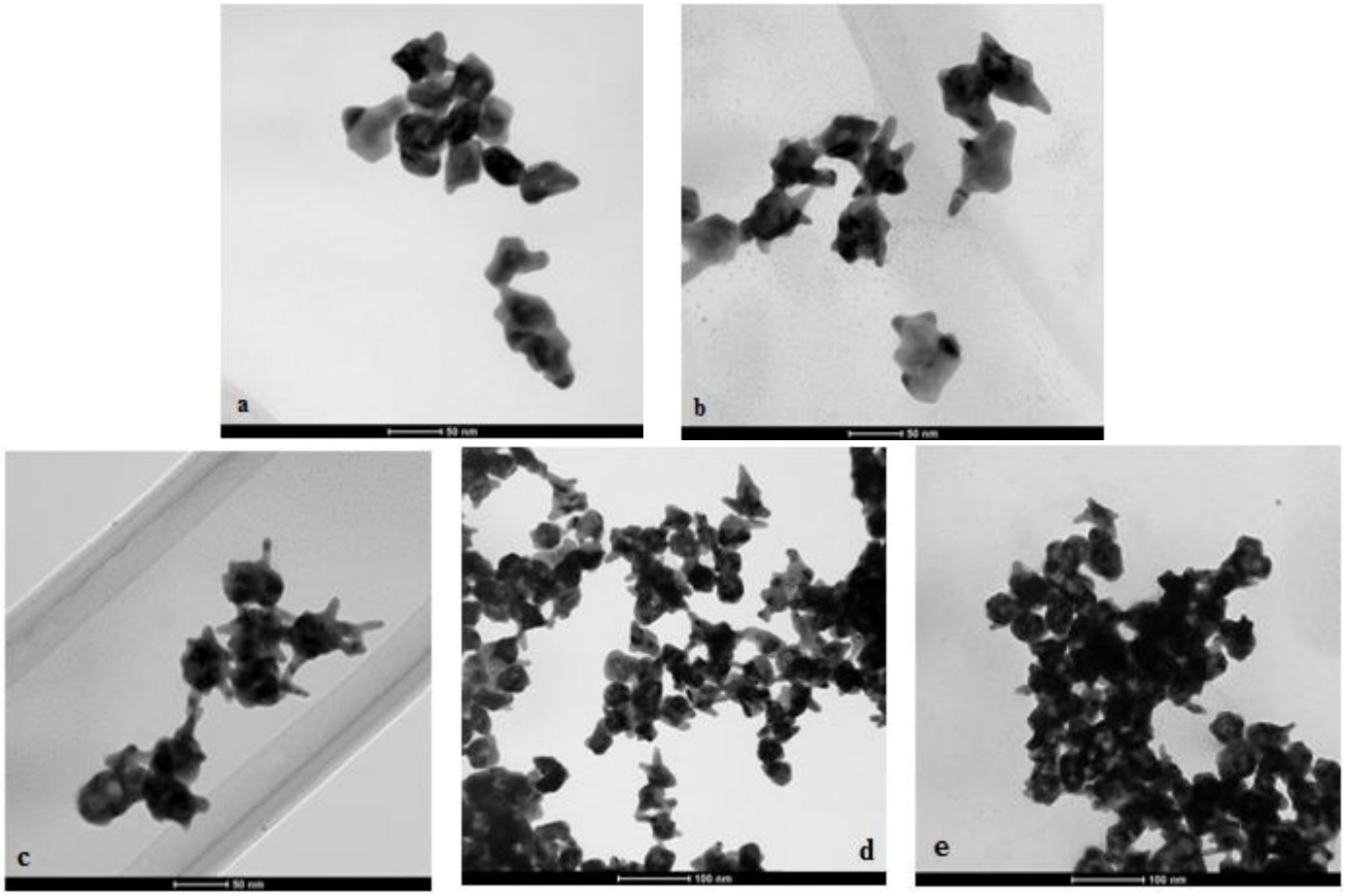


**Figure 4-11:** TEM images of anisotropic gold nanostructures synthesized at different molar ratios (S) of F-68 and high concentration of silver spherical seeds: a) S = 1.4; b) S= 5.6; c) S = 11.3; d) S= 22.7 and e) S = 45.4.

Figure 4-11 shows the evolution of the morphology by TEM from irregular shapes at low concentrations of F-68 (Figure 4-11a) to nanoparticles with short-length branches at intermediate concentrations (Figure 4-11b-c) and finally more aggregated pseudo-spherical shapes for the highest ratios of copolymer (Figure 4-11d-e). These nanostructures have an average size comprised between 40 - 60 nm and a medium number of branches between 3 and 5 with an average length of 10 - 25 nm depending on the synthesis conditions. However, at higher levels of copolymer, (figures 4-11d and 4-11e) the size and number of branches start to decrease.

From the Vis-Near Infrared spectra evaluated, it arises that there is an optical correlation between the sizes, the number of branches and the aggregation state observed in the series. The localized surface plasmon maximum evolves from 600 nm to up to 790 nm for the intermediate S ratio of 11.3 (see Figure 4-12) corresponding to the morphology with a higher number of branches (Figure 4-11c). The trend evolves back to 600 nm probably due to the reduction in size and thorns. (Figure 4-11d-e).

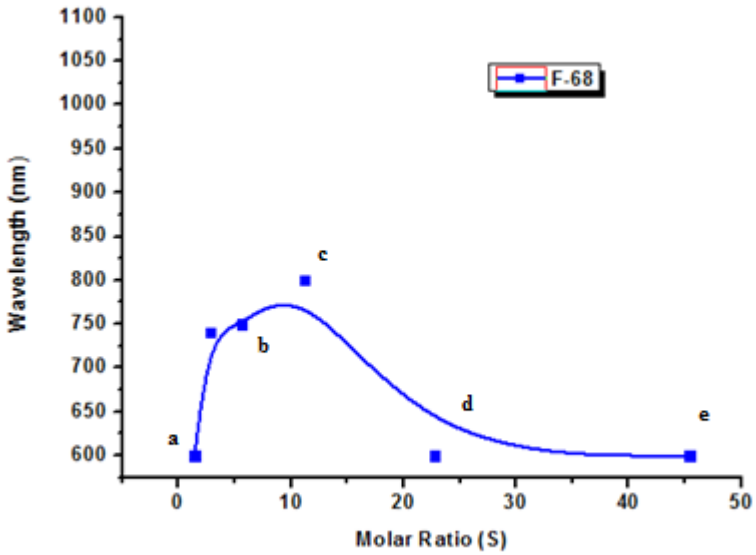


**Figure 4-12**: Evolution of the maximum absorbance obtained for increasing F-68 copolymer concentrations and high concentrations of silver seeds.

Therefore, we can assume that a major influence in the formation of star-shaped gold nanoparticles is attributed to the copolymer F-68, in comparison with the F-127 counterpart even in the presence of high concentrations of silver seeds.

### 4.2.2. Experiments with low concentration of silver seeds and Pluronic F-68 as copolymer

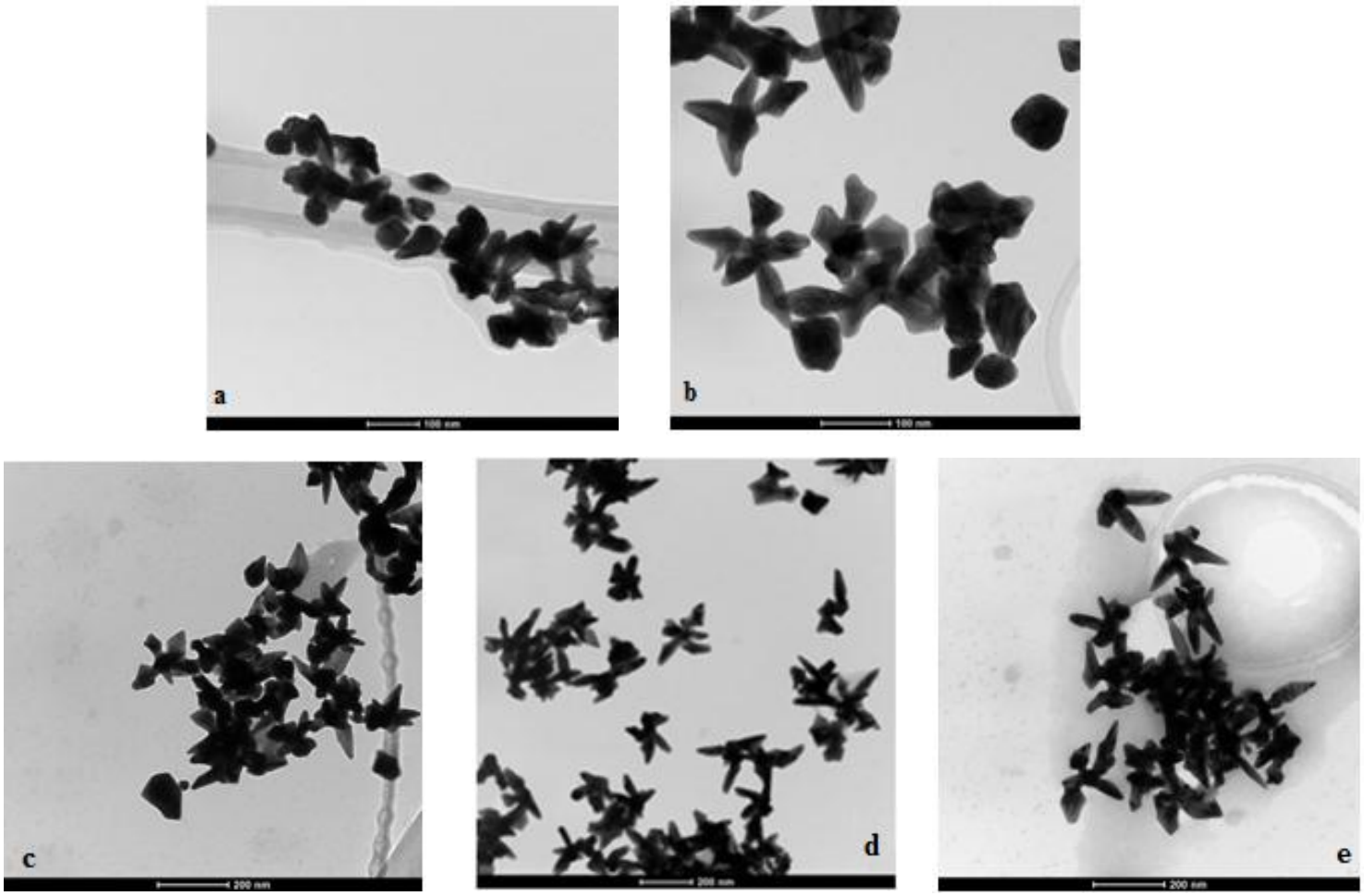


**Figure 4-13:** TEM images of anisotropic gold nanostructures synthesized at different molar ratios (S) of F-68 and low concentration of silver spherical seeds: a) S = 70.9; b) S= 141.9; c) S = 283.8; d) S = 567.7 and e) S = 1135.4.

The group of TEM images shown in Figure 4-13 clearly put in evidence the impact of F-68 and how the resulting morphologies gradually vary from irregular bipyramids to multi-branched structures. It is also worth mentioning that a combination of both structures is observed until intermediate copolymer concentrations are employed (Figure 4-13b-c). Additionally, the average sizes of these branches is closed to 60-70 nm and are considerably wider than previous structures obtained with F-127. Interestingly, these branches are also featured with a more triangular-pyramidal shape than other structures.

The evolution in the morphology of the nanostructures synthesized is also reflected in the localized surface plasmons absorption recorded by UV-Vis. Figure 4-14 shows the systematic red-shift detected in the maximum absorption bands as the molar ratio increases.

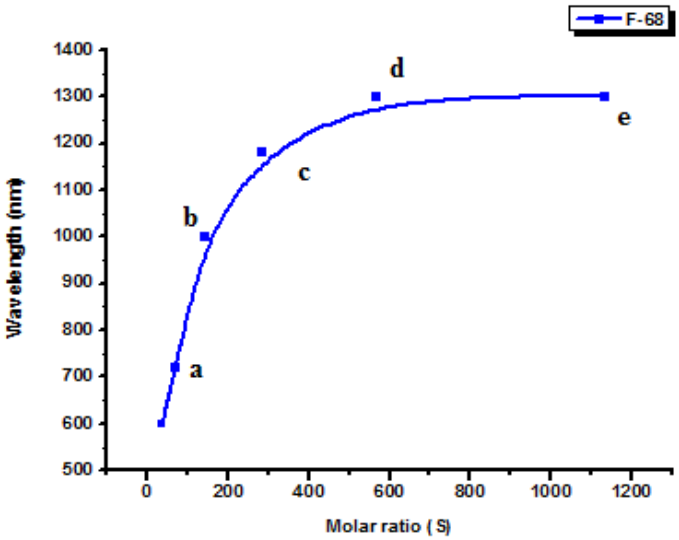


**Figure 4-14**: Evolution of the maximum absorbance obtained for increasing F-68 copolymer concentrations and low concentrations of silver seeds.

This series represents a good example on the efficiency of the copolymer for tuning the morphology and optical response from 600 nm to 1300 nm, thereby spanning the Vis-NIR window that it is useful for a wide variety of biomedical and sensing applications. In this particular series is also worth showing the UV-Vis absorbance spectra corresponding to several F-68 / silver seeds ratios into further detail (Figure 4-15).

Although the maximum surface plasmons at higher wavelengths are progressively red-shifted following the trend depicted in Figure 4-14, the presence of an additional maximum centered at 520-540 nm cannot be neglected, for the lower S ratios (see figure 4-15).

This signal stems for the transversal plasmonic response of the bipyramid-shaped branches and the irregularly shaped nanoparticles coexisting with the nanostars (see Figure 4-13b-c). As the copolymer concentration rises up, the maximum is red-shifted above 1000 nm coinciding with more homogeneous size distributions as shown in Figure 4-13d-e.

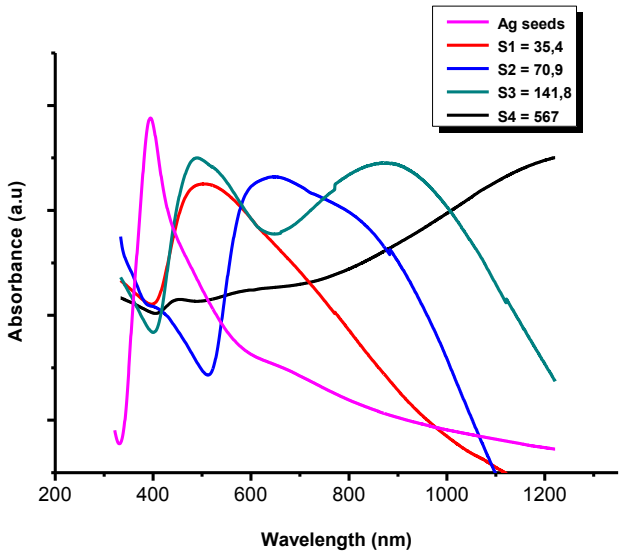


**Figure 4-15:** Absorption curves for different molar ratios

### 4.2.3. Discussion of the results obtained with F-68

- ***Influence of silver seeds concentration:***

An analogous influence is observed in comparison with the F-127 copolymer. The presence of a major number of nucleation sites (i.e. major number of initial silver seeds) facilitates the formation of smaller gold nanostructures and vice versa.

- ***Influence of the copolymer concentration:***

For both series of syntheses carried out with F-68 in the presence of high and low concentration of silver seeds (Figures 4-11 and 4-13), there is a clear evolution of the morphology at different copolymer concentrations accompanied by a gradual red-shift in the localized surface plasmons (Figures 4-12 and 4-14). This evolution does not exist in the case of reactions carried out with F-127 (Figures 4-3 and 4-5) in which all the nanostructures synthesized at different copolymer concentrations remain very similar in size and shape until the CMC is reached. Conversely, the CMC threshold for F-68 is not reached at room temperature and a continuous evolution is observed in the branching morphology without incurring in the formation of external micelles.

The presence of pseudo-aggregates with no sharp branches in the series at high levels of silver in conjunction with the simultaneous formation of nanostars and irregular shapes under certain experimental conditions is suggesting that the complex formed by CTAB and F-68 is not as stable as the CTAB-F127 system. Only in a short range of molar ratios (from 2.8 to 11.3 ) at high seed concentration stable CTAB-F-68 complexes are formed, as a consequence of that there is an increment in size and anisotropy. Moreover, the retarded evolution of the maximum surface plasmon absorptions is also suggesting that the lower presence of PEO-PPO subunits (intrinsic to the chemical nature of F-68) diminishes the reduction capacity of gold by PEO and the stability onto the gold surfaces provided by the PPO (T. Sakai et al. 2007). For that reason, the trend is clearly visible for F-68.

## 4.3. REACTIONS CARRIED OUT IN THE PRESENCE OF PLURONIC P-104

In this section, similar experimental conditions have been taken into account but using P-104 as copolymer. If compared with F-127, this copolymer has a similar CMC at room temperature (T. Sakai et al. 2007). The main difference relies on the PEO:PPO ratio. Pluronic F-127 has 100:70 units, whereas P-104 has 27:61. Therefore, a different packing stabilization of the CTAB-P104 is expected and a different reducing behavior can be envisioned.

### 4.3.1. Experiments with high concentration of silver seeds and Pluronic P-104 as copolymer

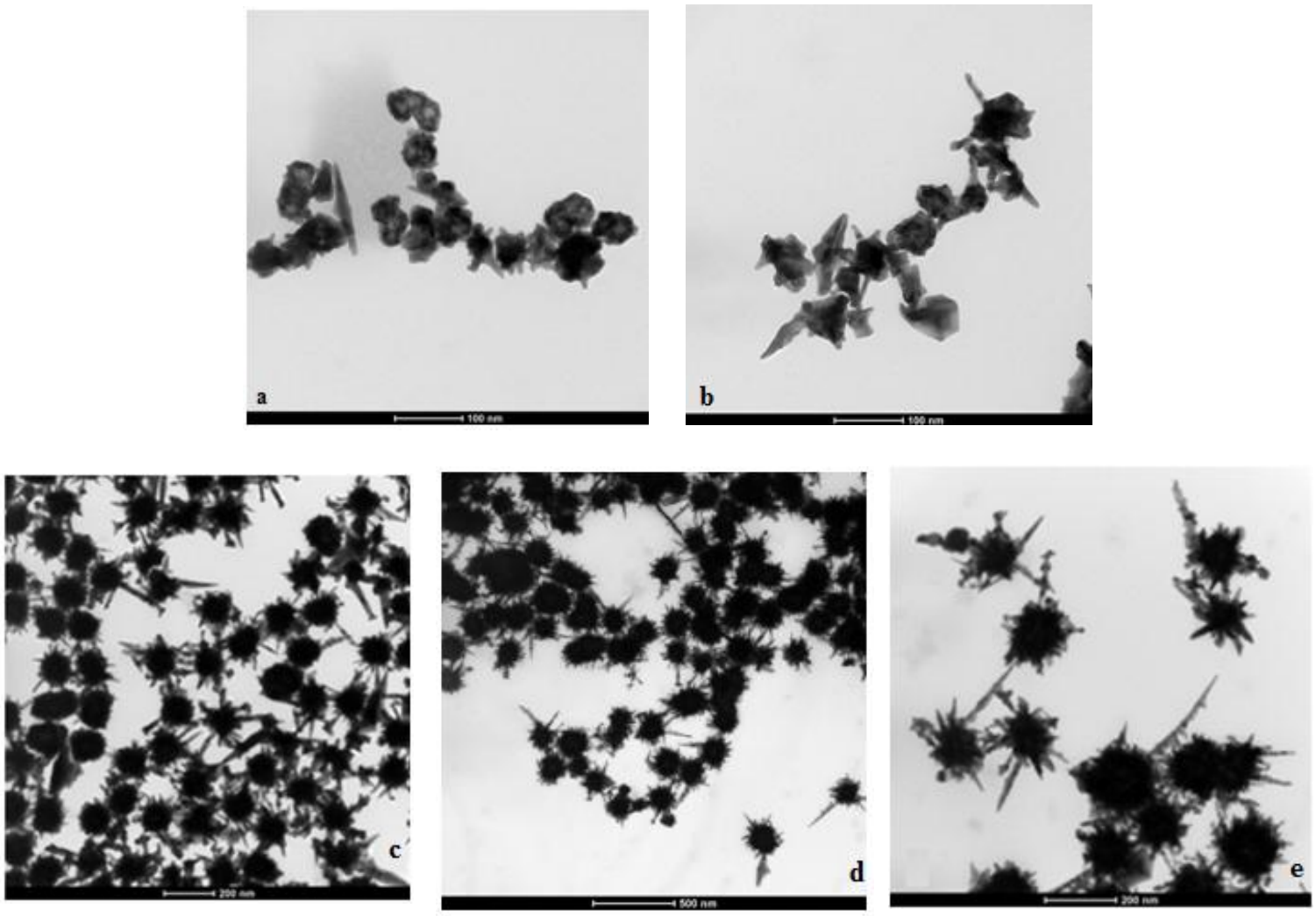


**Figure 4-16:** TEM images of anisotropic gold nanostructures synthesized at different molar ratios (S) of P-104and high concentration of silver spherical seeds: a) S = 1.4; b) S= 2.8; c) S = 11.3; d) S= 22.7 and e) S = 45.4.

The use of increasing concentrations of Pluronic P-104 while keeping a constant and high concentration of silver seeds yields a plethora of morphologies from pseudo-hollow spheres (Figure 4-16a) to thorny nanostars (Figure 4-16c-d) and finally, irregular snowflakes with multiple and long thorns obtained at higher concentrations of P-104 (Figure 4-16e). Moreover, the thorns exhibit an increment in number and length and the central parts of the nanostructures have a tendency to expand from 120 to 200 nm as the molar ratio S increases (Figure 4-16c-e).

Contrary to F-127 or F-68 copolymers, there is a clear evolution in the morphology that is further corroborated by the continuous red-shift of the Vis-NIR spectra and their corresponding surface plasmon maxima (see Figure 4-17 and 4-18 respectively). The thorny nanoparticles cover the 600-1100 nm NIR window, that is, the transparent window for tissues. Therefore, these nanostructures have a strong potential for applications in medicine imaging and biomedical sciences (see Applications section). The presence of hot spots at the tips of the thorns enables them as SERS candidates. (E. C. Le Ru et al. 2011) and (Khoundry and Vo-Dinh, 2008)

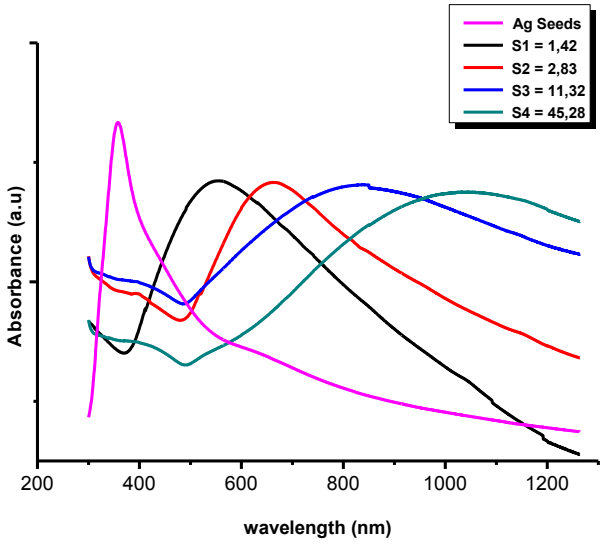


**Figure 4-17:** Absortion curves for different molar ratios

This increment in size is shown in the plasmonic study, small nanoparticles have their maximums of absorption at lower wavelengths. Conversely, the thorny nanoparticles with bigger sizes and major presence of sharp branches (c, d and e) tend to absorb at higher wavelengths. We can see a clear direct relationship (almost linear) between the molar ratio S and the maximum of absorption in Figure 4-18. This series represents another example of how the localized surface plasmon can be tuned and shifted from lower to higher wavelengths depending on the expected application.

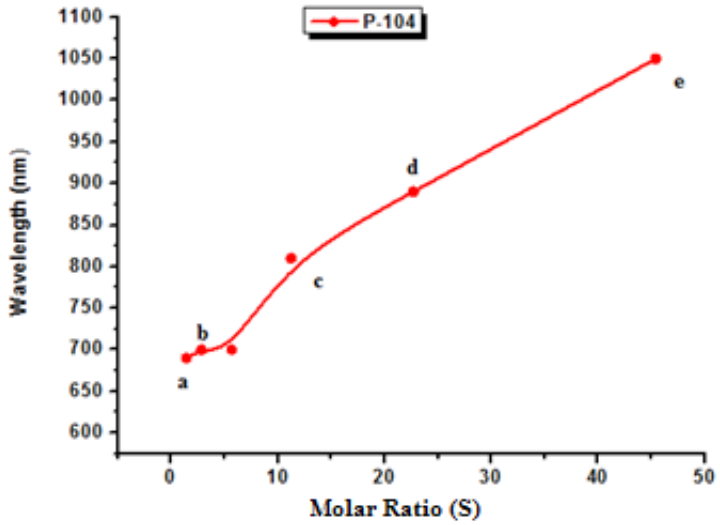


**Figure 4-18**: Evolution of the maximum absorbance obtained for increasing P-104 copolymer concentrations and high concentrations of silver seeds.

### 4.3.3. Experiments with low concentration of silver seeds and Pluronic P-104 as copolymer

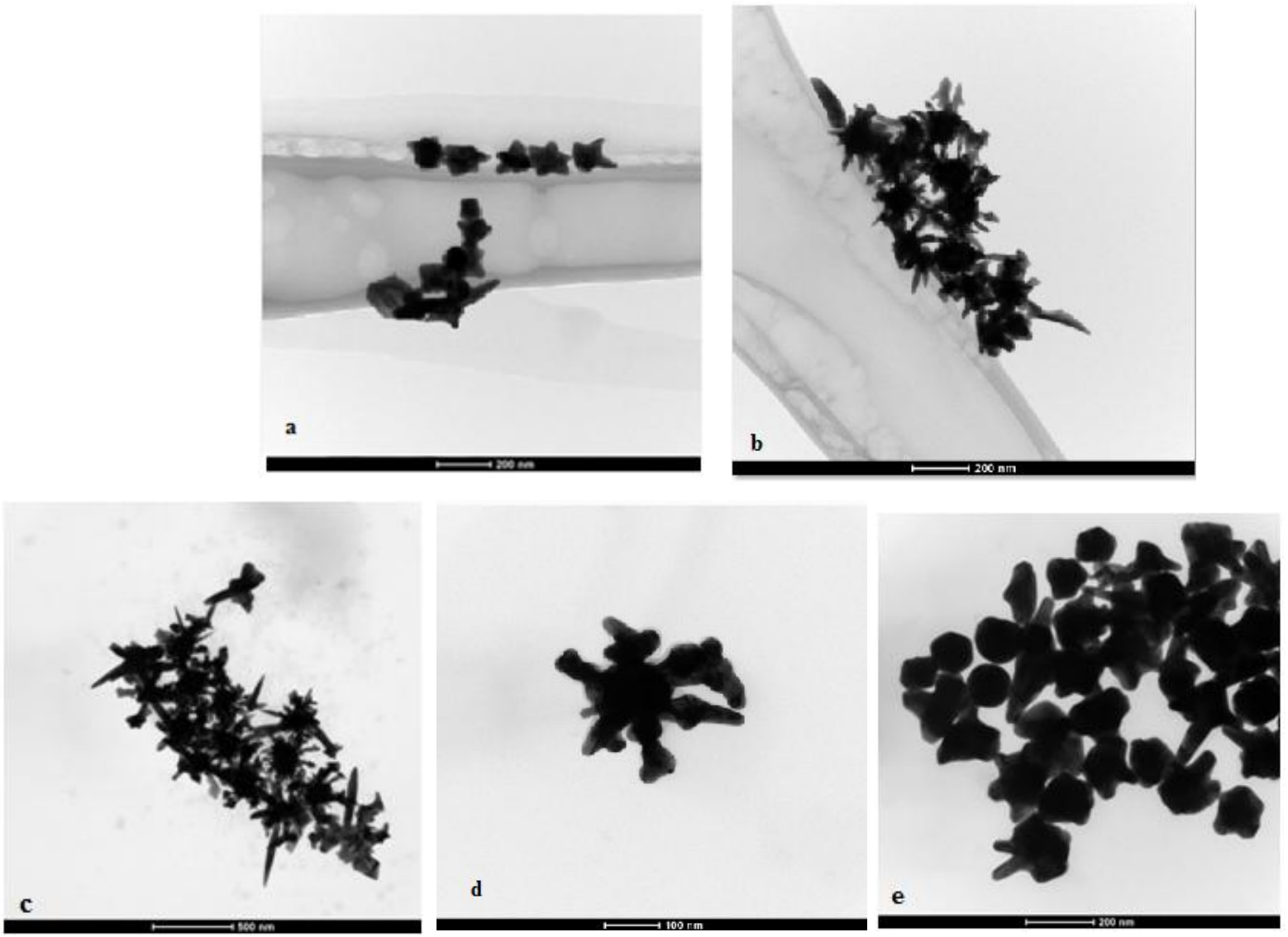


**Figure 4-19:** TEM images of anisotropic gold nanostructures synthesized at different molar ratios (S) of P-104 and low concentration of silver spherical seeds: a) S = 35.5; b) S= 141.9; c) S = 283.8; d) S = 567.7 and e) S = 1135.4.

Contrary to the previous series, the sequence of increasing the P-104 copolymer concentration is not so straightforward in the presence of low concentrations of silver seeds. In this case, the TEM images collected in Figure 4-19 show a great heterogeneity in shapes, sizes and morphologies. We can appreciate small not branched structures at low concentrations of P-104 (Figure 4-19a). At intermediate values, there seems to be certain tendency to form branched nanostructures with multiple lengths and an irregular central conformation (Figure 4-19b-c). Increasing the concentration of P-104 has the

opposite effect as we approach to the CMC threshold, since the gold nanostructures reduce their aspect ratio considerably (Figure 4-19d-e). The majority of the particles are similar or bigger than 100 nm and when the concentration of P-104 is increased, rounded particles bigger than 200 nm are also formed in combination with randomly distributed gold nanostars (Figure 4-19d-e).

These changes in the morphology are associated to the corresponding optical response detected by Vis-NIR absorption analysis. Multiple shapes and big sizes contribute to surface plasmon absorptions between 700-800 nm (see Figure 4-20). The continuous increasing shift up to 1000 nm is due to the bigger size of the nanostructures.

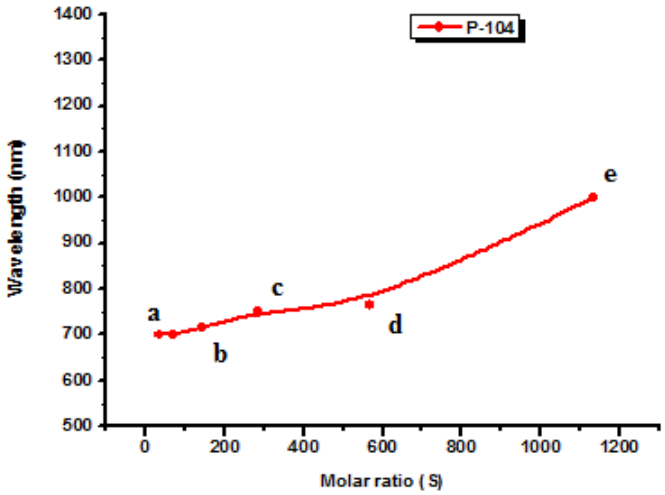


**Figure 4-20**: Evolution of the maximum absorbance obtained for increasing P-104 copolymer concentrations and low concentrations of silver seeds.

These changes in the morphology are associated to the UV-Vis absorption analysis. There is not a big increment in the maximum of absorption in the 5 first syntheses, all of them are between 700 and 780 nm however the maximum of the last synthesis (e) is shifted to 1000 nm due to the bigger size of the nanostructures.

### 4.3.3. Discussion of the results obtained with P-104

***- The influence of silver seed concentration:***

As previously discussed for the series containing F-127 and F-68 triblock copolymers, there is a clear influence on the final size of the obtained gold nanostructures and bigger nanoparticles are observed when a lower number of nascent nuclei is present (a lower concentration of starting silver seeds is used). It is also remarkable, that at higher concentrations of silver seeds, that is, in the presence of a major number of nucleation sites, there seems to be a more homogeneous control of the overall sizes and shapes. The formation of thorny gold nanoparticles with an expanded central snowflake-like morphology looks very similar to the previously reported gold nanostars synthesized by Yuan et al. (H. Yuan & W. Ma 2011) (Figure 4-21). In their work, the authors claimed that the formation of long thorns was governed by the presence of AgCl as previously described in the F-127 discussion section. Herein, it is plausible that the shorter number of PEO units in the P-104, retards the reduction process of gold and the subsequent formation of AgCl. Therefore, the growth of additional and secondary branches can be favored yielding the final thorny nanostructures observed.

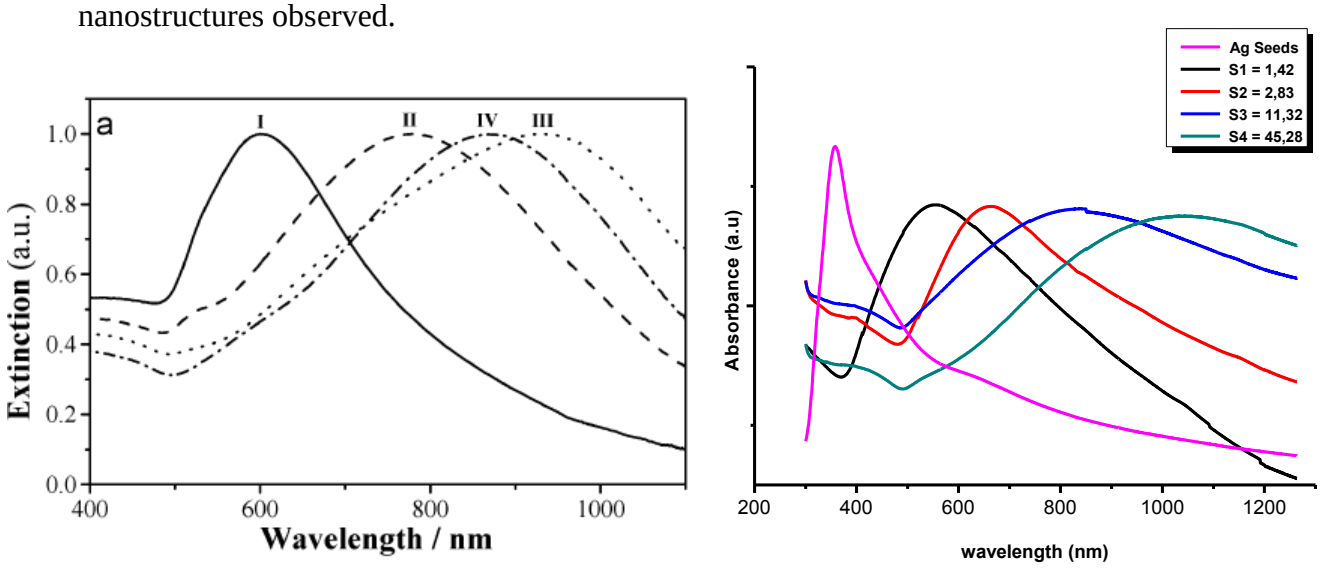


**Figure 4-21:** UV-Vis absorption spectra corresponding to the thorny gold nanoparticles synthesized by Yuan et al. (H. Yuan et al. 2011) (left) and our experimental results (right)

***- The influence of copolymer concentration:***

The impact of P-104 is clearly demonstrated both in the evolution of morphology and the corresponding optical response. The increment of P-104 favors the presence of an increasing number of sharp branches (thorns) and the progressive red-shift of the localized surface plasmons from 670 - 1100 nm depending on the molar ratio.

Similarly to F-127, the formation of micelles containing individual gold nanoparticles of 1-2 nm is also observed as the CMC of P-104 is reached (see Figure 4-22) thereby yielding pseudo-spherical gold nanoparticles which reduce their mean size. Likewise, it is worth mentioning that the lower presence of PEO units inherent to the chemical nature of P-104 seems to form a really stable surfactant-copolymer complex with CTAB with certain flexibility to induce multiple branching growth as the presence of silver seeds or P-104 concentration are increased.

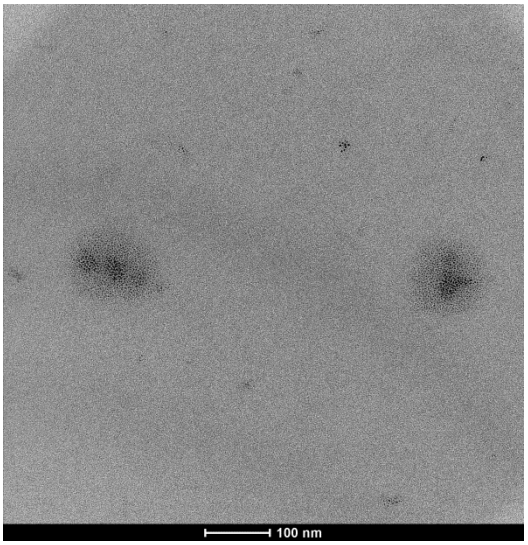


**Figure 4-22:** TEM image of a micelle formed during a synthesis carried out with a high concentration of copolymer Pluronic P-104 and low pseudo-spherical seed concentration

## 4.4. REACTIONS USING SILVER NANOCUBES AS SILVER SEEDS

In the following experiments we have replaced silver seeds by silver nanocubes and we have repeated the syntheses showed in section 4.3 with Pluronic P-104 as copolymer. The concentration of silver added is the same as in the previous series and the nanocubes have a size between 50 and 70 nm. The motivation to use silver nanocubes relies on their more homogeneous size dispersity, their lower mean diameter and the evaluation of the possible influence of using seeds with a well-known crystalline facet exposed to the reaction media. Pluronic P-104 is selected because of the good tunability results obtained for silver seeds and described in section 4.3.

### 4.4.1. Experiments with high concentration of silver nanocubes and Pluronic P-104 as copolymer

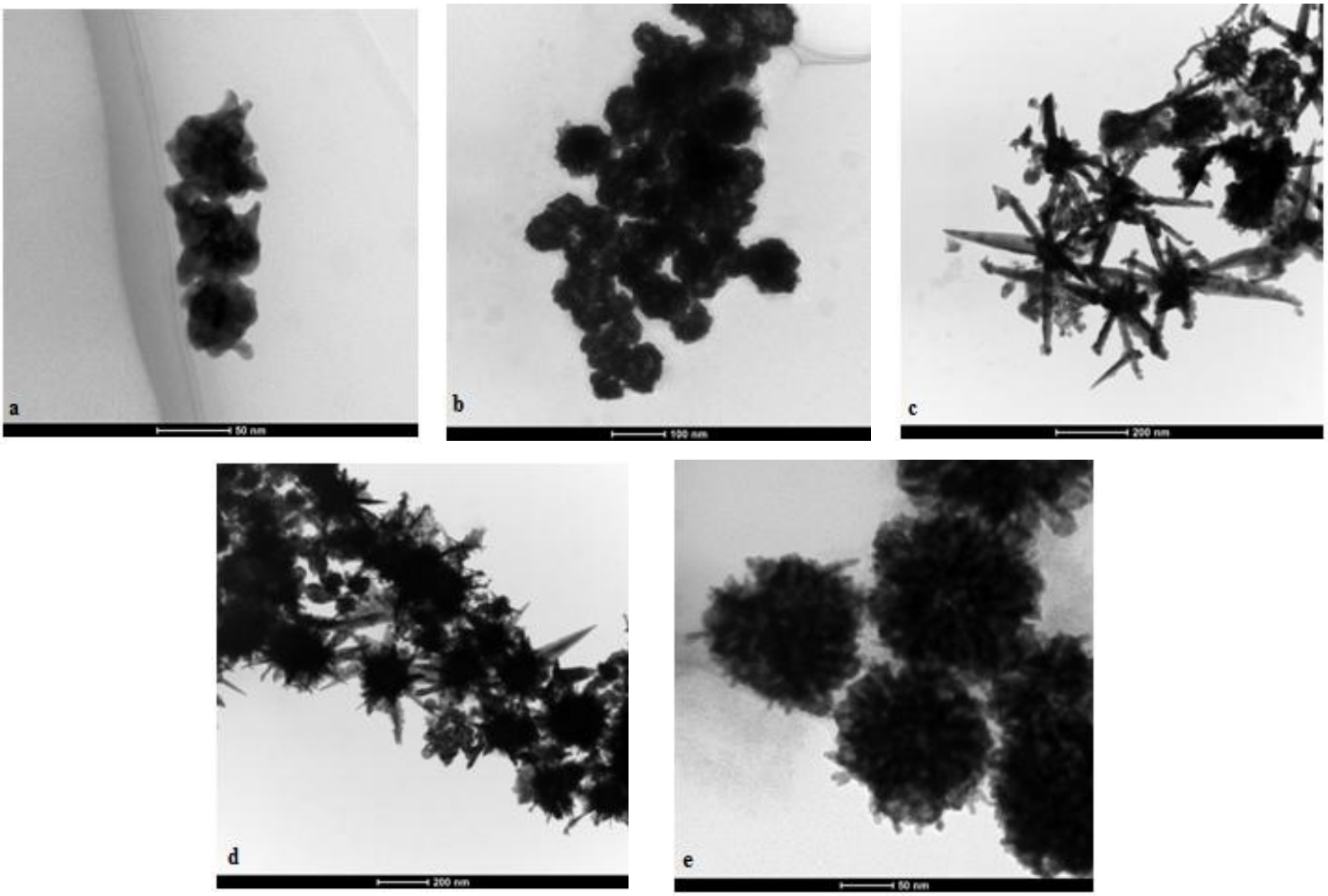


**Figure 4-23:** TEM images of anisotropic gold nanostructures synthesized at different molar ratios (S) of P-104 and high concentration of nanocubes: a) S = 1.4; b) S= 2.8; c) S = 11.3; d) S= 22.7 and e) S = 45.4.

Figure 4-23 shows the corresponding TEM images of gold nanostructures obtained in the presence of increasing P-104 concentrations. If we analyze carefully the figures, we can appreciate that in Figure 4-23a-c, there is an increment of the size which is directly related with the amount of P-104 added. However, as in the previous case when a concentration threshold of copolymer P-104 is reached, a drastic change in the morphology is observed from nanothorns with a more limited anisotropy (Figure 4-23d) to hollow snowflakes with 70 nm in size (Figure 4-23e).

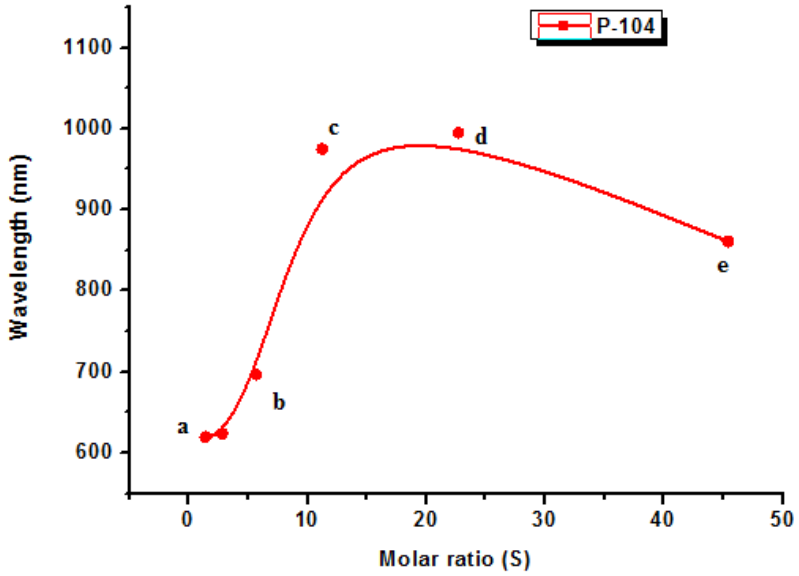


**Figure 4-24**: Evolution of the maximum absorbance obtained for increasing P-104 copolymer concentrations and high concentrations of silver nanocubes

As previously described for the experiments carried out in the presence of F- 68 and P-104, there is an important change in the optical properties that are tailored to the morphology, size and shape of gold nanoparticles. There is a maximum at 980 nm in Figure 4-24c-d associated to the sharpest thorny nanostructures. The reduction observed when the CMC is reached can be attributed to the reduction in size of the snowflake-like structure formed in conjunction with the presence of hollow dendrites (Figure 4-24e). This latter structure posses a surface plasmon oscillation located at 860 nm that provides an excellent possibility for bio-applications given the added value of its average diameter (70-80 nm).

### 4.4.2. Experiments with low concentration of silver nanocubes and Pluronic P-104 as copolymer

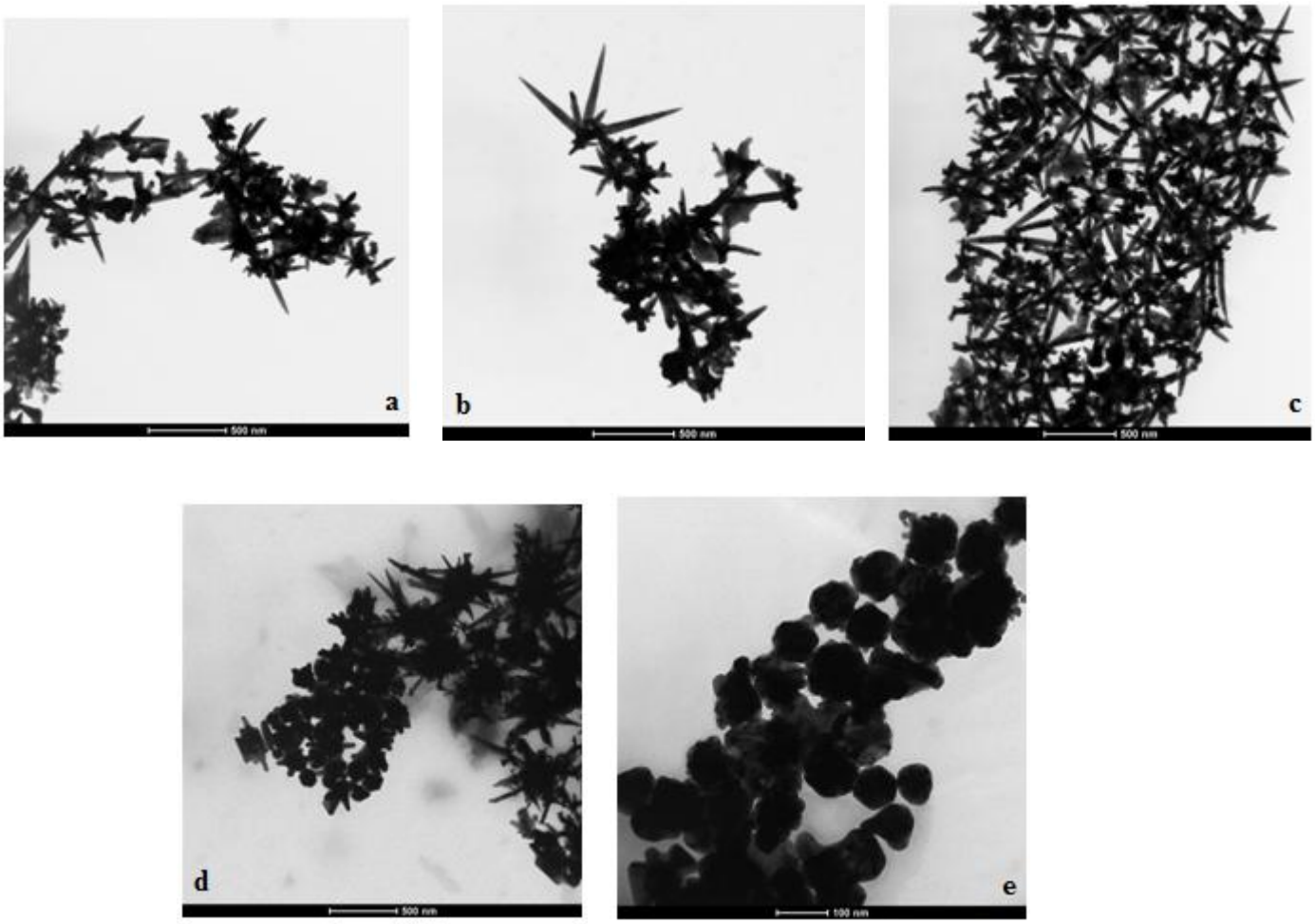


**Figure 4-25:** TEM images of anisotropic gold nanostructures synthesized at different molar ratios (S) of P-104 and low concentration of silver nanocubes: a) S = 35.5; b) S= 70.8; c) S = 141.9; d) S = 567.7 and e) S = 1135.4.

Figure 4-25 shows a similar trend in the change of morphologies elucidated by TEM as the amount of P-104 increases in the presence of a much lower concentration of silver nanocubes. Herein, the average mean length of branches is closed to 200 nm (Figures 4-25a, 4-25b and 4-25c) and corresponds to the maximum tip-enhancement of the surface localized plasmonic oscillations at 1200-1300 nm (Figure 4-26). The reduction of the maximum absorbance to 800 nm is again associated to the self-micellar organization of P-104 which inhibits the formation of a stable CTAB-copolymer complex.

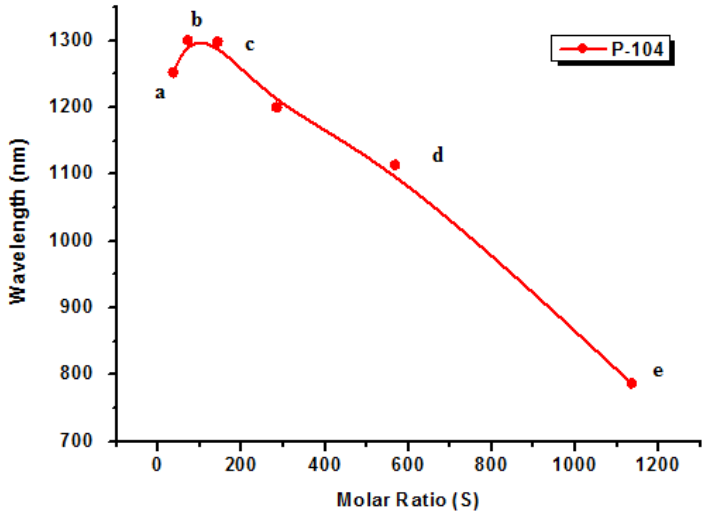


**Figure 4-26** Evolution of the maximum absorbance obtained for increasing P-104 copolymer concentrations and low concentrations of silver nanocubes

This evolution in morphology is summarized in the trend of the Vis-NIR of the maximum absorption spectra where at low molar ratios, the nanoparticles absorb at high wavelengths, which is in accordance with their branched morphology As it was expected, there is a decrease in the maximum of absorption at high S due to the smaller size and reduced aspect ratio of the nanoparticles synthesized at higher P-104 concentrations.

### 4.4.3. Discussion of the results obtained employing silver nanocubes as seeds and P-104 as copolymer:

- ***Influence of P-104 as copolymer:***

The role of P-104 as co-directing agent that influences the morphology and optical response of the formed nanoparticles is identical to the previously discussed section where pseudo-spherical silver seed were employed. (section 4.3.3) Due to their low CMC (T. Sakai et al. 2007) micelles are formed at high copolymer concentrations diminishing the size and anisotropy degree of the resultant gold nanostructures, as a consequence of that there is a shift to high energetic frequencies (lower wavelengths) at high molar ratios in both group of syntheses.

- ***Influence of Silver Nanocubes:***

In terms of seed concentration, the same trends can be observed for high and low concentration of silver nanocubes if compared with their spherical counterparts. Bigger sizes accompanied by red-shifting to higher wavelengths and higher branching probabilities are observed in the presence of lower concentration of cubes where the dominant role of the copolymer is imposed. As a main difference with respect to previous syntheses, it is worth mentioning that great homogeneity in sizes obtained for most of the experimental conditions carried out with silver nanocubes.

# 5. APPLICATIONS

## 5.1. Surface-Enhanced Raman Spectroscopy (SERS)

### 5.1.1. Introduction to SERS

Surface-enhanced Raman scattering is a powerful tool for the analysis of vibrational information of analyte molecules and with sufficient sensitivity to provide single-molecule detection (S. Nie and S Emery 1997). Therefore, it constitutes a relevant and important technique for sensoring applications. This technique relies on collective oscillations of conduction electrons in metals, which interact with light to produce high confinement of electromagnetic energy, particularly in narrow gaps between metal nanoparticles, but also at sharp nanoscaled corners and edges. These localized surface plasmons can convey great intensity enhancement factors which directly translate into an increase of the electronic transition probabilities of atoms or molecules exposed to such fields.

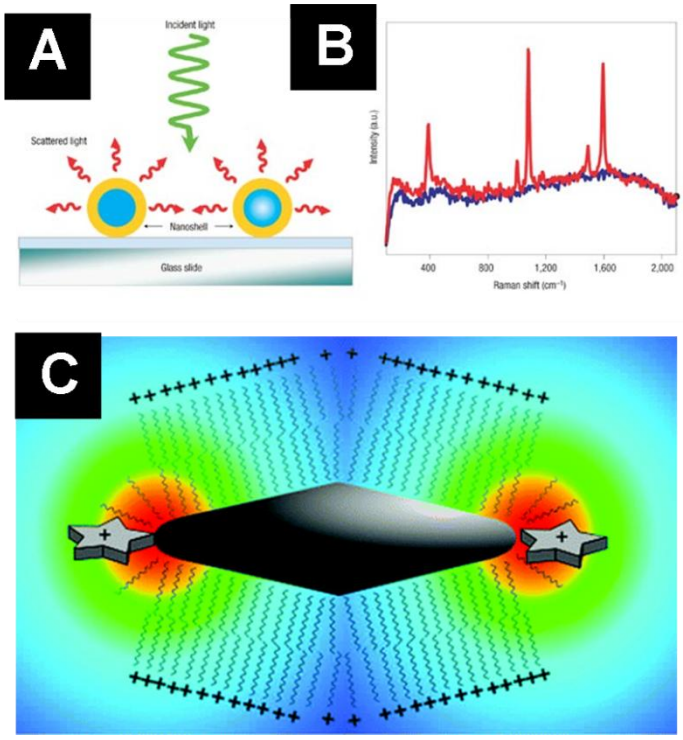


**Figure 5-1:** Examples of gold nanoshells (a) and gold bipyramids (b) used for SERS detection of target molecules. (b) Typical SER spectrum where the Raman signal intensity of a target molecule with low Raman cross section is amplified in the presence of active metal hot spots provided by sharp metal edges.

SERS is the result of two main types of enhancement in the Raman signal response:

**i) Electromagnetic enhancement.** It can be attributed to a modification and enhancement of the local electromagnetic field E. It takes into account the interaction of the incident laser beam with irregularities on the metal surface such as metal micro-particles, roughness profile or sharp tips. It is believed that the laser light excites conduction electrons at the metal surface leading to a surface plasma resonance and strong enhancement of electric field E. The presence of these collective electrons multiplies the Raman response (see Figure 5-1).

**ii) Chemical enhancement.** The second enhancement is caused by the enhancement of the polarizability of the target molecule under study and may occur because of a charge-transfer effect or chemical bond formation between metal surface and molecules under observation.

The most popular and universal substrates used for SERS are electrochemically etched silver electrodes as well as silver and gold colloids with average particle size below 20 nm. More recently, the use of gold nanoshells (S. Lal et al 2007), gold bipyramids (E. C. Le Ru et al. 2011) and gold nanostars (L.Rodriguez-Lorenzo et al. 2009) and (P.S. Kumar et al. 2008) with sharp tips is becoming a promising alternative for high sensitive detection of target (bio)-molecules.

### 5.1.2. Experimental Set up

Raman detection was performed using a Jobin-Yvon Labram HR800 Raman microscope with a linearly polarized 647 nm laser line, a 20 x 0.4 NA Leica objective, 5 mW power and 45 seconds of acquisition time. The experimental setup was modified to carry out the Raman experiments directly in ethanol solution. Different colloidal suspensions containing the selected gold nanostars in ethanol were sonicated in the presence of different Rhodamine 6G ethanolic solutions prepared at $10^{-5}$ and $10^{-7}$ M concentrations and used as target molecule with low Raman cross-section (see Figure 5-2). The intermixing process was maintained for 5-10 minutes prior to the Raman analysis.

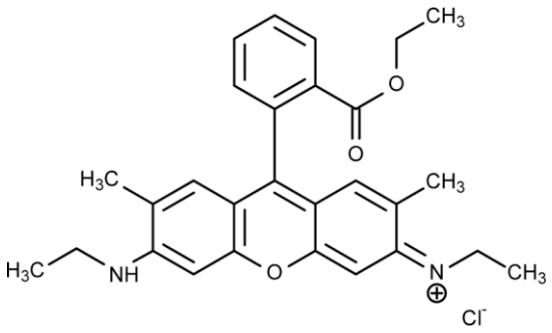

**Figure 5-2**: Chemical structure of Rhodamine 6G

### 5.1.3. Results on selected samples

It is important to note that the reported values are for isolated particles in solution, and care has been taken to limit aggregation. Therefore, the presence of additional hotspots normally promoted by aggregation is prevented and the SERS effect is less plausible than in normal backscattering experiments carried out onto solid substrates[1]. Moreover, the selected dye lacks of chemical interaction with gold nanostars and only an electromagnetic enhancement can be envisioned.

Figure 5-1a and 5-1b show TEM images of the morphology of nanostars synthesized in the presence of F-127, using high concentration of spherical silver seeds (section 4.1.1). This sample was selected because of the presence of multiple branch tips and the good dispersion observed in the sample. Figure 5-3c also shows the corresponding UV-Vis spectrum with a localized surface plasmon maximum at ca. 620 nm, which nearly overlaps the incident laser excitation wavelength used for the experiments ($\lambda$ = 633 nm).

As it is shown in figure 5-3c, a clear Raman signal enhancement is observed for concentrations of $10^{-5}$ M of dye and a series of intense Raman modes associated to in-plane C-C streaching vibrations are clearly detected. Lowering the detection limit by 2 orders of magnitude did not render any relevant signal different to the blank experiment carried out in the presence of nanostars without Rhodamine 6G (see Figure 5-3d). Additional samples were checked without a significant SERS response (data not shown). The shift between the laser excitation source wavelength and the maximum plasmon absorption are the main reasons attributed to the lack of response detected in other samples.

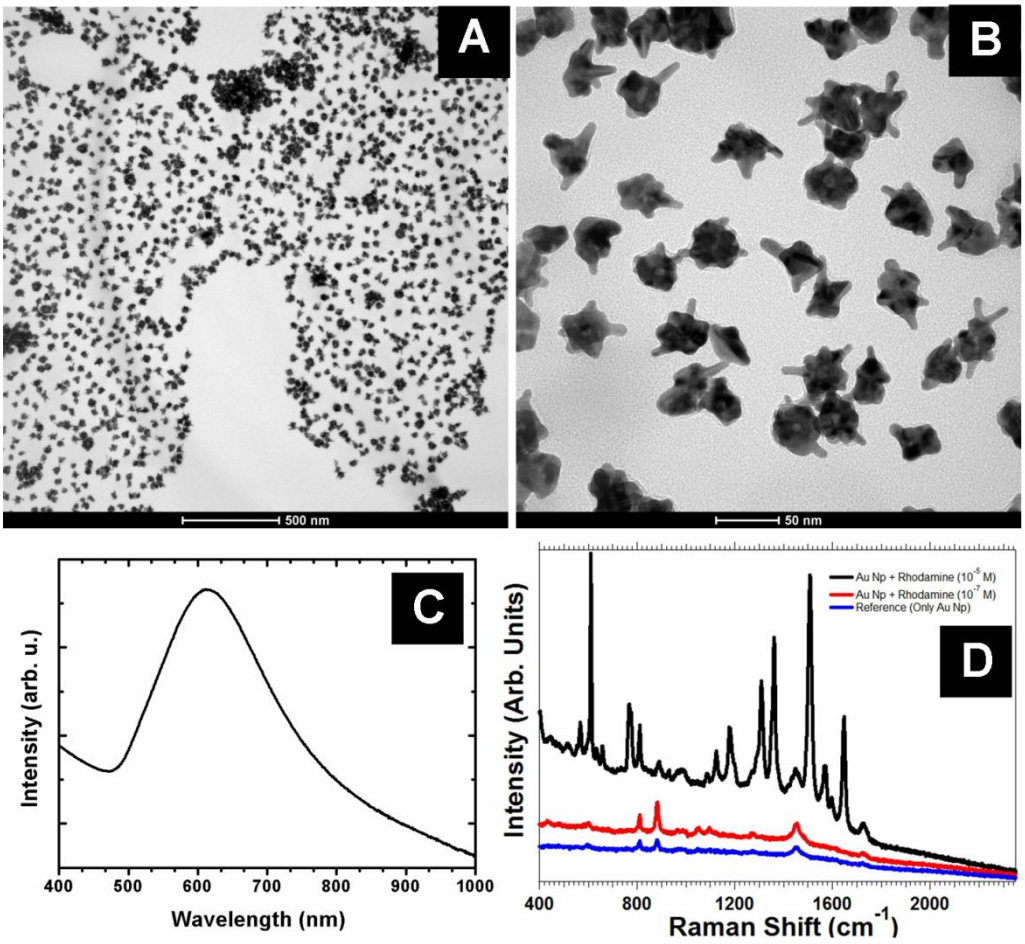


**Figure 5-3:** a-b) TEM images at different magnifications corresponding to gold nanostars synthesized in the presence of F-127 and 500 uL of spherical silver seeds; c) UV-Vis spectrum corresponding to the selected nanostars; d) Surface-enhanced Raman signals of R6G at $10^{-5}$ M (black spectrum) and $10^{-7}$ M (red spectrum) in the presence of nanostars and the corresponding blank experiment in the absence of dye (blue spectrum).

## 5.2. OPTICAL HYPERTHERMIA IN THE NIR AND CYTOTOXICITY VIABILITY EXPERIMENTS

### 5.2.1. Introduction to Optical Hyperthermia

The term hyperthermia refers to an artificial phenomenon that makes the temperature of the body increase or just a particular region of it. It is a heat application technique in the treatment of cancer. Besides apoptosis, hyperthermia induces a reduction of blood flow and blood vessel density that favors hypoxia, acidosis and energy deprivation (Hildebrandt, Wust, et al. 2002). Hyperthermia as a cancer treatment technique can be applied by different kinds of energy such as microwaves, radiofrequency, ultrasound, and hot surfaces as resistive wire implants and nanoparticles (Chichel, Skowronek, et al 2007).

The nanoparticles used for hyperthermia can be magnetic or resonant in the near infrared region NIR (800 - 1200 nm). The behavior of magnetic nanoparticles is influenced by a magnetic field and resonant nanoparticles are heated up by infrared radiation. The energy used belongs to the near infrared region because organism tissues do not absorb that incident light and moreover, hemoglobin and water have their lowest absorbance coefficient between 650 and 900 nm (Weissleder 2001). Likewise, a tissue irradiated by a laser in that range will not increase its temperature. However, if resonant nanoparticles are placed inside the tissue the laser irradiation would induce cellular death.

It has been demonstrated that NIR light can penetrate at least 10 cm across chest tissues and 4 cm across the skull to the brain as well as 4 cm across muscles using microwatt power laser (class 1 according with the classification of the “Food and Drug Administration (FDA) of USA) (Ntziachristos et al. 2000). Therefore, phototherapy by NIR laser can be applied in superficial and inside tumors.

It is possible to place the nanoparticles close to the tumor by two different ways, the passive and the active targeting (Danhier, Ucakar, et al. 2010). The passive targeting is based on the enhanced permeation and retention effect (EPR), nanoparticles designed with the required size enter the tumor by its vasculature and then accumulate in certain

solid tumors. In the active targeting, nanoparticles are engineered by surface functionalization with biomolecules which attach tumor-specific cell markers.

### 5.2.2. Experimental set up

The experimental work was carried out at the Institute of Nanoscience of Aragón (INA). This study consists on heating and specific kind of nanoparticles synthesized before, by the use of a laser of 808 nm of wavelength and measure the increment of the temperature of the sample. In order to avoid the temperature changes at the work place, all the laser-experiments are carried out in an incubator with a temperature control.
*The experimental setup used for photothermal heating experiments is detailed in Appendix I, at the end of the manuscript*

The experiments showed in this work were performed irradiating the sample with a continuous laser source of 808 nm. It is important to take into account that the results obtained with this technique are influenced by the volume solution used as well as the laser -sample distance and the power of the laser. In order to compare different results, the laser irradiation tests were always performed in a similar way (see figure 5-4). The same class of vial was used in any case, the laser power was 100% (2 W) and the volume of sample used was 2 mL. The distance between the sample and the laser was 3 cm.

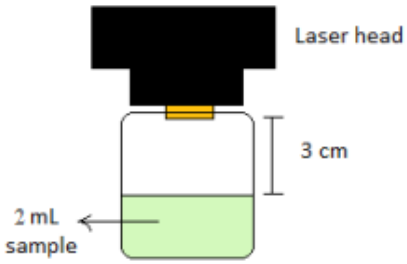


**Figure 5-4:** Scheme of the sample position for laser irradiation experiments

As it has been explained before, not all nanoparticles can be used for optical hyperthermia, only the ones that have the maximum of absorption around 808 nm are useful. However, this is not the only condition; nanoparticles require a reproducible synthesis, be stable, homogeneous and have the possibility of be scaled up at high volumes.

After revising these conditions, and searching among all our kind of nanoparticles synthesized, we chose the following nanostructure obtained in the presence of P-104 due to the position of the surface plasmonic absorption centered at 800 nm and the size ranged below 150 nm, two requisites of paramount importance for hyperthermia (V. Cebrián, L.Gomez Et al. 2012) and (Jin Z.Zhang Et al 2008)

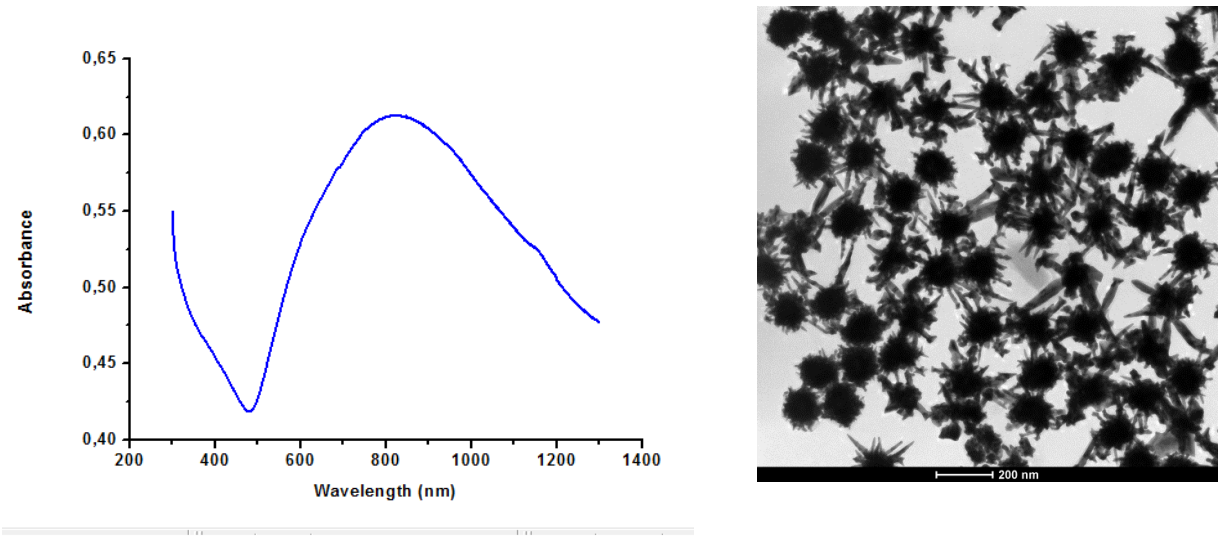


**Figure 5-5**: TEM Image (right) and UV-Vis spectra (left) of the nanoparticles employed in photothermal test

In the first laser-induced heating test, we have measured the increment of temperature of the solvent, as control experiment (water in this case) and the increment of temperature of 2 different samples whose gold nanothorns concentrations are 0,25 and 0,45 mg/mL.

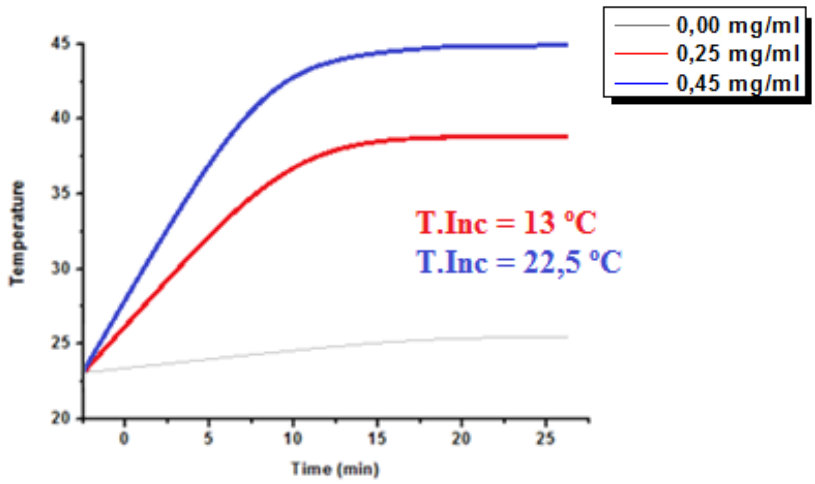


**Figure 5-6:** Increment of temperature at different nanoparticles concentration

As we can appreciate in Figure 5-6, there is an increment of 22.5 ºC in the sample with the higher concentration of gold nanostars and an increment of 13 ºC in the sample with the concentration at 0.25 mg $mL^{-1}$. Although water has a really low absorbance coefficient at 808 nm, the increment of water temperature in 1,5 ºC cannot be ruled out.

Once the heating capacity of the selected gold nanostars was confirmed at the NIR window, the citotoxicity was also evaluated. As we know, we have employed CTAB in the synthesis process, which is a very well-known cytotoxic compound. Other important problem is the non-stability of the nanoparticles when the toxic surfactant is removed. In order to solve both problems, we have carried out a dialysis process followed by a polyethyleneglycol (PEG) coating process according to the protocol developed by Maltzahn and co-workers (Maltzahn et al. 2009).

After coating the gold nanoparticles with PEG, the optical properties and heating capabilities of the coated were measured again in order to check if the coating process had affected the system. The main results of the Vis-NIR absorption and the temperature profiles are depicted in Figure 5-7.

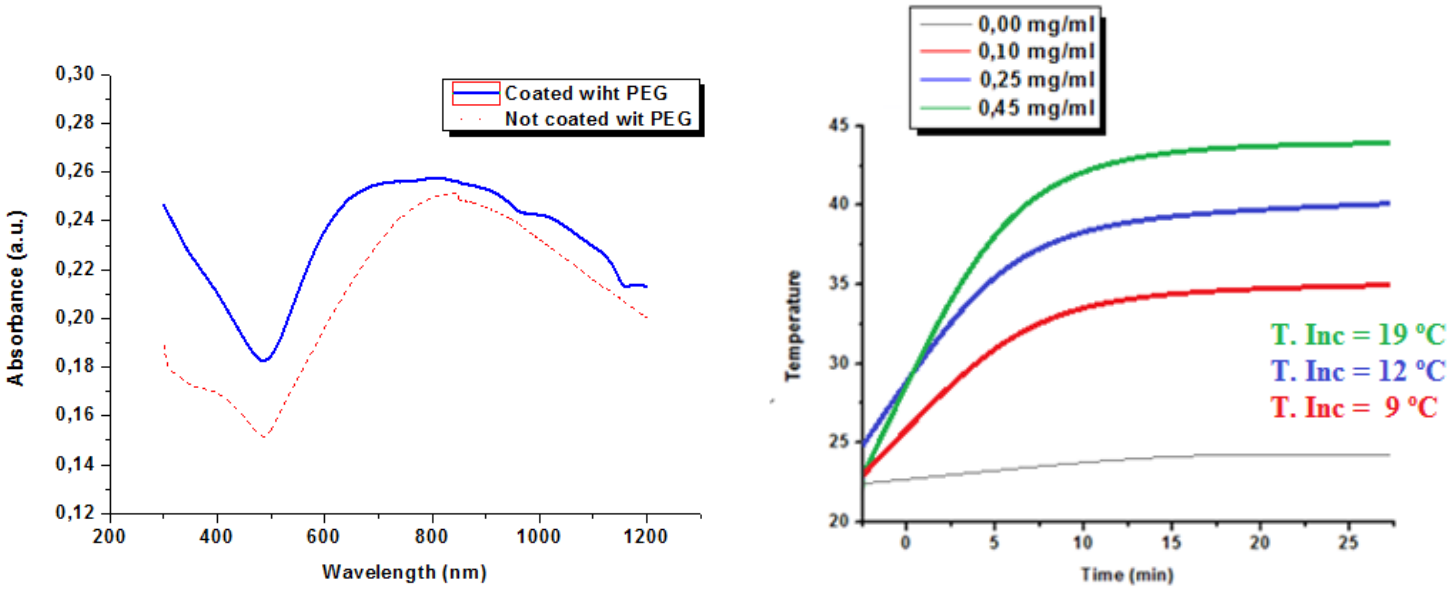


**Figure 5-7:** UV-Vis absorption curve of particles coated with PEG and without PEG (left), and increment of temperature at different PEG coated nanoparticles concentration upon irradiation with a laser excitation wavelength of 808 nm and a power of 2 W (right).

As we can appreciate in figure 5-7, nanoparticles coated with PEG have a similar UV-Vis absorption curve. The curve is a bit wider, it can be due to the evolution of the morphology of the nanoparticles because both absorption curves were made with a 21 days of difference. In the case of laser tests, there are not big differences between the increments of temperature obtained with particles coated with PEG and the experiments carried out with particles not coated with PEG.

### 5.2.3. Toxicity/Viability Studies

Alamar blue Viability studies were carried out at the Hospital Miguel Servet in Zaragoza in collaboration with Maria del Mar Encabo. In these studies, first of all it is necessary to add different concentrations of the selected gold nanoparticles (from 0.01 to 0.1 mg/mL) to a U251MG cell culture (a type of brain tumoral cells). After that, a known amount of resazurin, which is a non fluorescent agent, is added to a known amount of tumor U251MG cells. Once this compound is inside the cell, it is reduced by the cell to resurfin (figure 5-8) which is a fluorescent molecule.

**Figure 5-8:** Resazurin reduction process to resurfin

Measuring the fluorescence at different times, (form 30 minutes to 7 days) we can calculate the number of living cells during this period of time because the fluorescence intensity produced is proportional to the number of living cells. All the Alamar blue viability process is shown in the following figure:

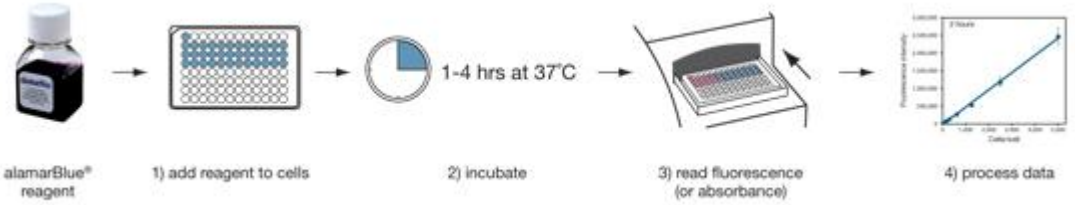


**Figure 5-9:** Alamar blue schematic measuring process. (Al-Nasiry, S. et al. 2007)

The toxicity/viability study results with tumor U251MG cells are summarized in Figure 5-10 for different PEGylated nanostar concentrations and incubation times:

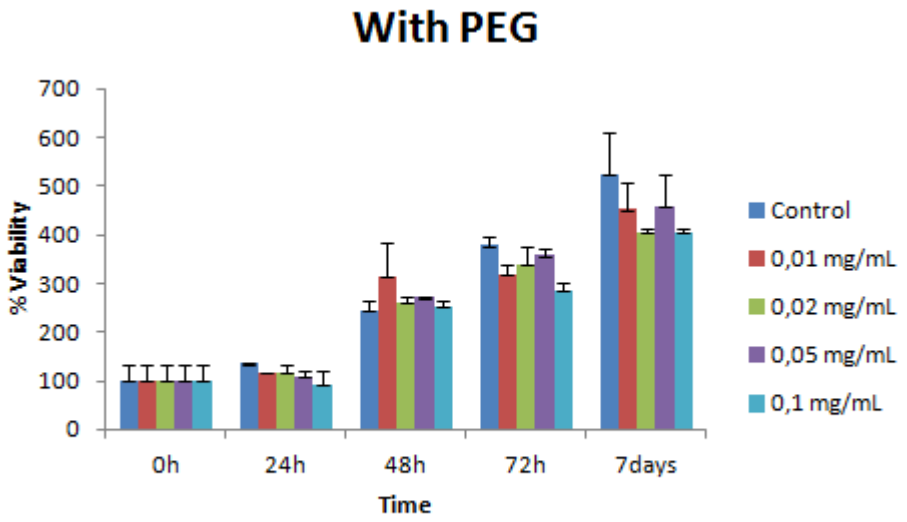


**Figure 5-10:** Toxicity/Viability study results obtained for the PEGylated nanostar selected at different concentrations and incubation times.

Analyzing the diagram, we can conclude that our gold nanoparticles coated with PEG, are not cytotoxic. As we can appreciate in figure 5-10, the number of viable cells increases along the 7 days of incubation following a similar trend to the control experiment.

### 5.2.4. Discussion of the results obtained for optical hyperthermia and cytotoxicity

***- Heating capability and PEGylation process***

We have selected a gold nanothorn synthesized in the presence of P-104 which fulfilled the initial requirements of maximum absorbance at 800 nm and reduced sizes (below 130 nm). Subsequently, the sample has been properly coated with PEG to improve the internalization capacity of the nanoparticles into the cellular system. Additionally, the heating capabilities of the samples before and after PEGylation was evaluated with a 808 nm laser, thereby yielding an increment of 10 ºC for a solution of 2 mL and a concentration of 0.1 mg $mL^{-1}$ which is in the same range of previously

reported gold nanoshells but below gold hollow nanospheres which yielded an increment almost 3 times higher (V. Cebrián , L.Gomez Et al. 2012).

***- Viability studies with brain tumoral cells:***

Although the preliminary studies of cytotoxicity carried out at the Hospital Miguel Servet are quite promising, there are still pending several assays to further confirm these results. The use of Confocal Microscopy to further confirm the internalization of the PEGylated nanostars is necessary and pending to be carried out. To date, only indirect measurements carried out by Raman have confirmed the presence of gold nanoparticles (data not shown) inside the cell membranes. Flow cytometry measurements will be also used to mark the nanostars and individually count them.

# 6. CONCLUSIONS

The combination of CTAB and different triblock copolymers like F-127, F-68 and P-104 yields stable complexes that act as co-directing agents and favor the anisotropic growth of gold nanostructures in the form of nanostars, thorny nanoparticles or pseudo-hollow snowflakes.

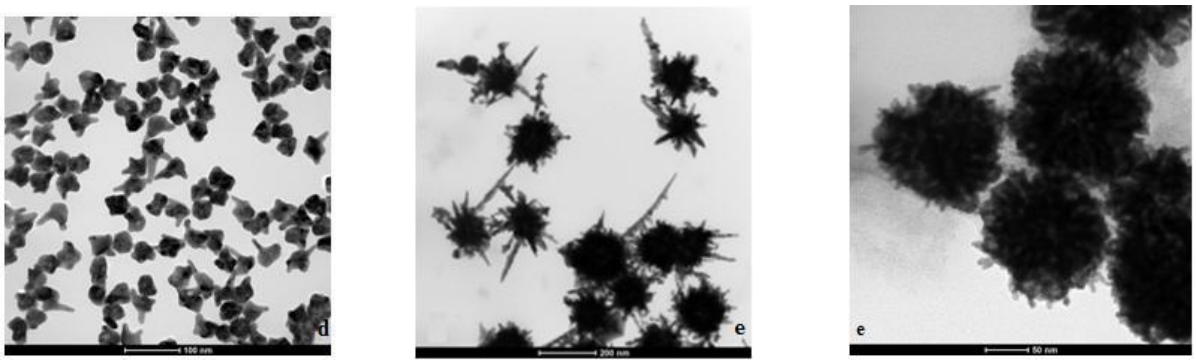


The initial concentration and shape of the seed growth solution containing silver nanostructures represents another critical synthesis parameter that strongly affects the final size and optical response of the resultant gold nanostructures.

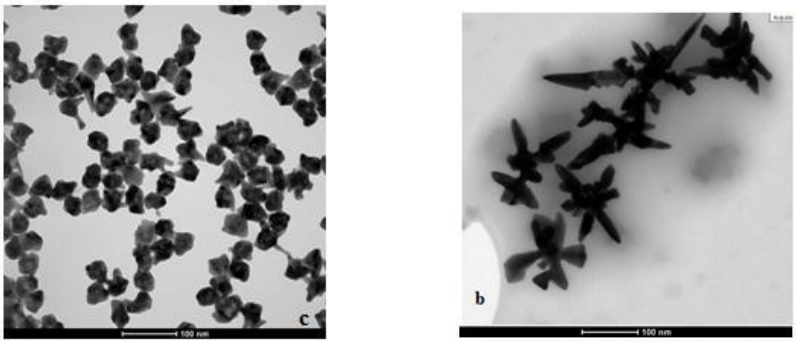


The reaction mechanism for the formation of anisotropic gold nanostructures is governed by the galvanic replacement of silver by gold in the presence of ascorbic acid, the subsequent formation of AgCl that affect the isotropic growth of the nanoparticles and also by the stability of the formed CTAB-Copolymer complex.

The presence of a lower number of PEO blocks in the selected copolymer minimize its reducing capacities, retards the formation of branches and permits a more controlled evolution of the branching and thorny structures.

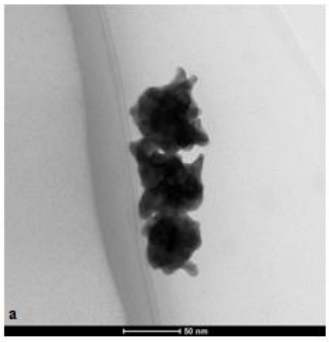


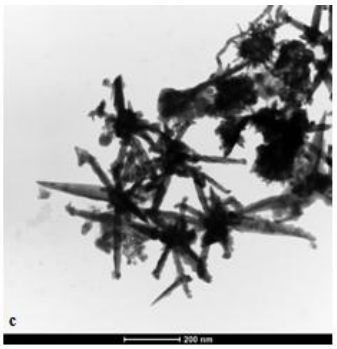


The proper selection of sizes and optical properties can render good candidates for SERS applications and photothermal applications. In our case, two different samples have been successfully tested: i) in the detection of a target dye molecule with limited Raman signal and ii) for NIR-laser-induced heating while keeping a reduced cytotoxicity in brain tumor cell cultures.

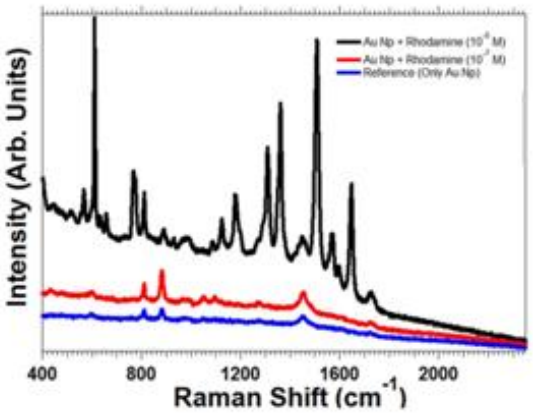


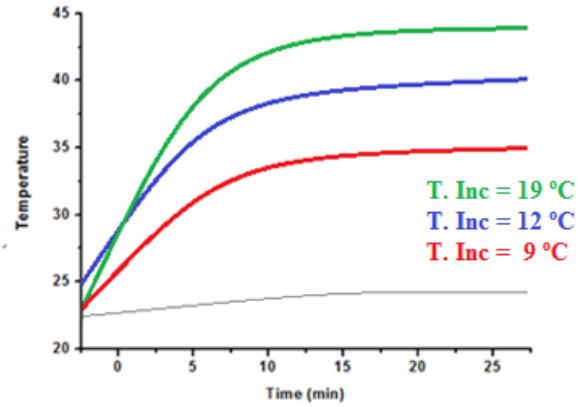


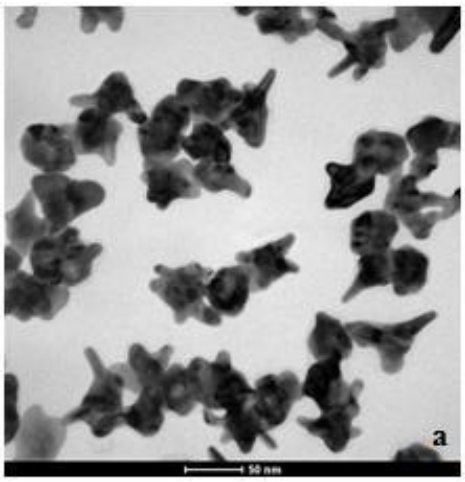


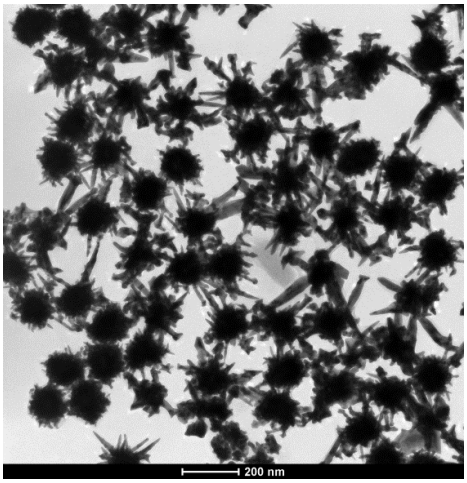

# REFERENCES:


Alvaro Mayoral, Cesar Magen, and Miguel Jose-Yacaman. *High-Yield Production of Long Branched Au Nanoparticles Characterized by Atomic Resolution Transmission ElectronMicroscopy.* Crystal Growth & Design 2011, 11, 4538–4543

Andrew M. Fales, Hsiangkuo Yuan, and Tuan Vo-Dinh. *Silica-Coated Gold Nanostars for Combined Surface-Enhanced Raman Scattering (SERS) Detection and Singlet-Oxygen Generation: A Potential Nanoplatform for Theranostics. Langmuir* 2011, 27, 12186–12190

Atwater, Harry A., Polman, Albert. *Plasmonics for improved photovoltaic devices.* Nature Materials (2010), 9(3), 205-213 CODEN: NMAACR; ISSN: 1476-1122.

Catherine J. Murphy, Tapan K. Sau, Anand M. Gole, Christopher J.Orendorff, Jinxin Gao, Linfeng Gou, Simona E. Hunyadi, and Tan Li. *Anisotropic Metal Nanoparticles: Synthesis, Assembly, and Optical Applications.* The Journal of the physical chemistry B. 2005, *109*, 13857-13870

Chichel A., Skowronek J., Kubaszewska M., Kanikowski M. *Hyperthermia – description of a method and a review of clinical applications*. Reports of Practical Oncology & Radiotheraphy 2007, 12, 267-275.

Christopher G. Khoury and Tuan Vo-Dinh. *Gold Nanostars for Surface-Enhanced Raman Scattering: Synthesis, Characterization and Optimization.* Journal of Physucal chemistry 2008, 112, 18849–18859

Colleen L. Nehl, Hongwei Liao, and Jason H. Hafner. (2006) *Optical Properties of Star-Shaped Gold Nanoparticles.* Nano Letters Vol. 6, Nº 4 , 683-688

Danielle K. Smith and Brian A. Korgel. *The Importance of the CTAB Surfactant on the Colloidal Seed-Mediated Synthesis of Gold Nanorods.* Langmuir 2008, *24*, 644-649

Danhier F., Ucakar B., Magotteaux N., Brewster M.E., Préat V. *Active and passive tumor targeting of a novel poorly soluble cyclin dependent kinase inhibitor*. International Journal of Pharmaceutics 2010, 392, 20-28.

Encai Hao, Ryan C. Bailey, George C. Schatz, Joseph T. Hupp, &S huyou Li. (2004). *Synthesis and Optical Properties of "Branched" Gold Nanocrystals.* Nano Letters Vol. 4, Nº 2 , 327-330

E. C. Le Ru, J. Grand, I. Sow, W. R. C. Somerville, P. G. Etchegoin, M. Treguer-Delapierre, G. Charron, N. Felidj, G. Levi and J. Aubard, *A Scheme for Detecting Every Single Target Molecule with Surface-Enhanced Raman Spectroscopy* Nano Letters., 2011, 11, 5013-5019.

Feng Hao, Yannick Sonnefraud, Pol Van Dorpe, Stefan A. Maier, Naomi J. Halas and Peter Nordlander. *Symmetry Breaking in Plasmonic Nanocavities: Subradiant LSPR Sensing and a Tunable Fano Resonance.* Nano Letters 2008 Vol. 8 No. 11 3983- 3988

Gordon, A., Lutz, G., Boninger, M., & Cooper, R. (2007). *Introduction to nanotechnology: Potential applications in physical, medicine and rehabilitation.* American Journal of Physical Medicine and Rehabilitation, 86, 225-241

Hildebrandt B., Wust P., Ahlers O., Dieing A., Sreenivasa G., Kerner T., Felix R., Riess H. *The cellular and molecular basis of hyperthermia*. Critical Reviews in Oncology hematology 2002, 43, 33-56.

Hsin-Lun Wu, Chiu-Hua Chen, and Michael H. Huang. *Seed-Mediated Synthesis of Branched Gold Nanocrystals Derived from the Side Growth of Pentagonal Bipyramids and the Formation of Gold Nanostar. Chemistry of Materials*. 2009, *21*, 110–114

Hong Yuan, Wanhong Ma, Chuncheng Chen, Huaiyong Zhu, Xueping Gao, and Jincai Zhao. *Controllable Synthesis of 3D Thorny Plasmonic Gold Nanostructures and Their Tunable Optical Properties.* The Journal of the Physical Chemistry C. 2011, 115, 23256–23260

Hong Yuan, Wanhong Ma, Chuncheng Chen, Huaiyong Zhu, Xueping Gao, and Jincai Zhao. *Shape and SPR Evolution of Thorny Gold Nanoparticles Promoted by Silver Ions.* Chemistry of Materials *Vol. 19, No. 7, 2007* 1597

L. Rodriguez-Lorenzo, R. A. Alvarez-Puebla, I. Pastoriza-Santos, S. Mazzucco, O. Stephan, M. Kociak, L. M. Liz-Marzan and F. J. G. de Abajo, *Zeptomol Detection Through Controlled Ultrasensitive Surface-Enhanced Raman Scattering.* Journal of the American Chemical Society, 2009, 131, 4616.

Muhammad Iqbal, Yong-Il Chung and Giyoong Tae. *An enhanced synthesis of gold nanorods by the addition of Pluronic (F-127) via a seed mediated growth process.* Journal of Materials Chemistry. 2007, 17, 335–342

Ntziachristos V., Yodh A.G., Schnall M., Chance B. *Concurrent MRI and diffuse optical tomography of breast after inddocyanine green enhancement*. Proceedings of the National Academy of Sciences USA 2000, 97, 2767-2772.

Paula C. Angelomé, Hamed Heidari Mezerji, Bart Goris, Isabel Pastoriza-Santos, Jorge Pérez-Juste, Sara Bals, & Luis M. Liz-Marzán (2012). *Seedless Synthesis of Single Crystalline Au Nanoparticles with unusual Shapes and Tunable LSPR in the near-IR.* Chemistry of Materials. 24, 1393−1399

Pandian Senthil Kumar1, Isabel Pastoriza-Santos1, Benito Rodríguez González, F Javie rGarcía de Abajo and Luis M Liz-Marzán. *High-yield synthesis and optical response of gold nanostars.* Nanotechnology 19 (2008) 015606.

P. S. Kumar, I. Pastoriza-Santos, B. Rodriguez-Gonzalez, F. J. Garcia de Abajo and L. M. Liz-Marzan. *Surface enhanced raman spectroscopy using Star-Shaped gold colloidal nanoparticles*. Nanotechnology, 2008, 19.

P. S. Kumar, I. Pastoriza-Santos, B. Rodriguez-Gonzalez, F. J. Garcia de Abajo and L. M. Liz-Marzan. *High-yield synthesis and optical response of gold nanostars.* Nanotechnology 19 (2008) 015606 (6pp)

Sihai Chen, Zhong Lin Wang, John Ballato, Stephen H. Foulger, and David L. Carroll. *Monopod, Bipod, Tripod, and Tetrapod Gold Nanocrystals.* Journal of the American chemical society 9 VOL. 125, NO. 52, 2003 16187

Sperling, Ralph A., Rivera Gil, Pilar, Zhang, Feng, Zanella, Marco, Parak, Wolfgang J. *Biological applications of gold nanoparticles.* Chemical Society Reviews (2008), 37(9), 1896-1908 CODEN: CSRVBR; ISSN: 0306-0012.

S. S. Al-Nasiry, N. N. Geusens, M. M. Hanssens, C. C. Luyten, R. R. Pijnenborg. *The use of Alamar Blue assay for quantitative analysis of viability, migration and invasion of choriocarcinoma cells.* Hum Reprod 22 (5) :1304-9 (2007), PMID 17307808

Tapan K. Sau and Catherine J. Murphy. *Room Temperature, High-Yield Synthesis of Multiple Shapes of Gold Nanoparticles in Aqueous Solution.* Journal of the American chemical society. VOL. 126, NO. 28, 2004 8649

Toshio Sakai and Paschalis Alexandridis. *Mechanism of Gold Metal Ion Reduction, Nanoparticle Growth and Size Control in Aqueous Amphiphilic Block Copolymer Solutions at Ambient Conditions.* Journal of Physical . Chemistry. B 2005, 109, 7766-7777

Weissleder R. *A clearer vision for in vivo imaging*. Nature Biotechnology 2001, 19, 316-317.

Zhang L., Gu F.X., Chan J.M., Wang A.Z., Langer R.S., Farokhzad O.C. *Nanoparticles in medicine: therapeutic applications and developments*. Clinical Pharmacology & Therapeutics 2008, 83, 761-769.

Zhang J.Z., Noguez C. *Plasmonic Optical properties and Applications of Metal Nanostructures*. Plasmonics 2008, 3, 127-150.